SANDIA REPORT SAND84-8233 • Unlimited Release • UC-62c
Printed July 1984

The Performance of High—Temperature Central Receiver Systems

P. De Laquil III and J. V. Anderson

Prepared by
Sandia National Laboratories
Albuquerque, New Mexico 87185 and Livermore, California 94550
for the United States Department of Energy
under Contract DE-AC04-76DP00789

SF 2900-Q(6-82)

Printed in the United States of America
Available from
National Technical Information Service
5285 Port Royal Road
Springfield, VA 22161

NTIS price codes
Printed copy: A04
Microfiche copy: A01

UC-62c

SAND84-8233
Unlimited Release
Printed July 1984

THE PERFORMANCE OF HIGH-TEMPERATURE CENTRAL RECEIVER SYSTEMS

Pascal De Laquil III
Solar Components Division
Sandia National Laboratories, Livermore

John V. Anderson
Thermal Systems and Engineering Branch
Solar Energy Research Institute
Golden, Colorado

ABSTRACT

The development of central receiver technology for the production of electricity is reasonably well established. One possible direction for future research and development efforts funded by the Department of Energy is high-temperature, high-performance systems. In this paper, the performance of central receiver systems is investigated for a range of heliostat sizes, field configurations, plant sizes, and receiver temperatures. The maximum plant efficiency achievable in a central receiver system that uses simple cavity geometry is shown for a range of receiver temperatures. The impact of changes in heliostat size, field packing density, and canting and focusing strategies on system efficiency are investigated over a range of plant sizes. The results of the study underscore the importance of accommodating high absorber plane fluxes in order to efficiently produce working temperatures at or above 1200^{o}C.

CONTENTS

ILLUSTRATIONS

TABLES

Summary

This study characterizes the high-temperature performance of solar central receiver systems that use simple cavity geometry. Three plant sizes were examined. The results indicate that although very high temperature systems (up to 2100°C) are achievable, the system efficiency* for converting sunlight to thermal energy decreases significantly as the receiver temperature increases. This decrease in system performance translates directly into a higher cost/performance ratio for high-temperature systems. Whether high-temperature systems are cost-effective is not addressed in this study.

To achieve high temperatures, high receiver peak fluxes must be accommodated. Due principally to the free convection thermal losses, cavity receivers operating at peak absorber fluxes of 0.25 MW/m^2 have relatively low efficiencies. Significant improvements in system efficiency can be achieved by increasing the peak absorber flux to 0.5 MW/m^2 for receiver temperatures up to 1200°C. For receiver temperatures greater than 1200°C, the maximum system efficiency increases monotonically up to the highest peak fluxes studied (1.8 MW/m^2).

There are three important points which should be kept in mind when the results of this study are considered. The first regards the temperature scale. An average absorber temperature of 600°C is approximately the state-of-the-art for water-steam and molten nitrate salt technologies; 900°C to 1200°C is the range proposed for the next generation of high-temperature receivers (DARTS, solid particle, etc.). Thus the performance values calculated for temperatures of 1500°C and above represent substantial projections from current technology.

The second point is that the results presented here are strongly based on a cavity receiver convective loss correlation proposed by Kraabel.** This correlation is based upon measurements taken in the most realistic laboratory-scale tests performed to date and is considered the best available model. However, the correlation has been only minimally validated against measurements taken on full-scale receivers. Furthermore, some uncertainty exists in regard to the correlation's applicability to receiver geometries with aperture-to-absorber surface area ratios greatly differing from those of the experimental cavities. Despite these concerns, the model represents the most directly applicable work done to date in this area and should be useful in predicting at least the trends associated with this phenomena.

---

* In this study, "system efficiency" represents the fraction of the sunlight incident on the heliostat which is converted to thermal energy at the receiver absorber surface and would be available to a working fluid.

** D. L. Siebers and J. S. Kraabel, "Estimating Convective Energy Losses from Solar Central Receivers," Sandia National Laboratories, SAND84-8717, April 1984.

Finally, it should be pointed out that these results apply to a simple open-aperture receiver. No attempt has been made to include the effects of such loss-reduction techniques as aperture windows, terminal concentrators, or volumetric receivers. Indeed, our results demonstrate the potential value of such devices at higher absorption temperatures.

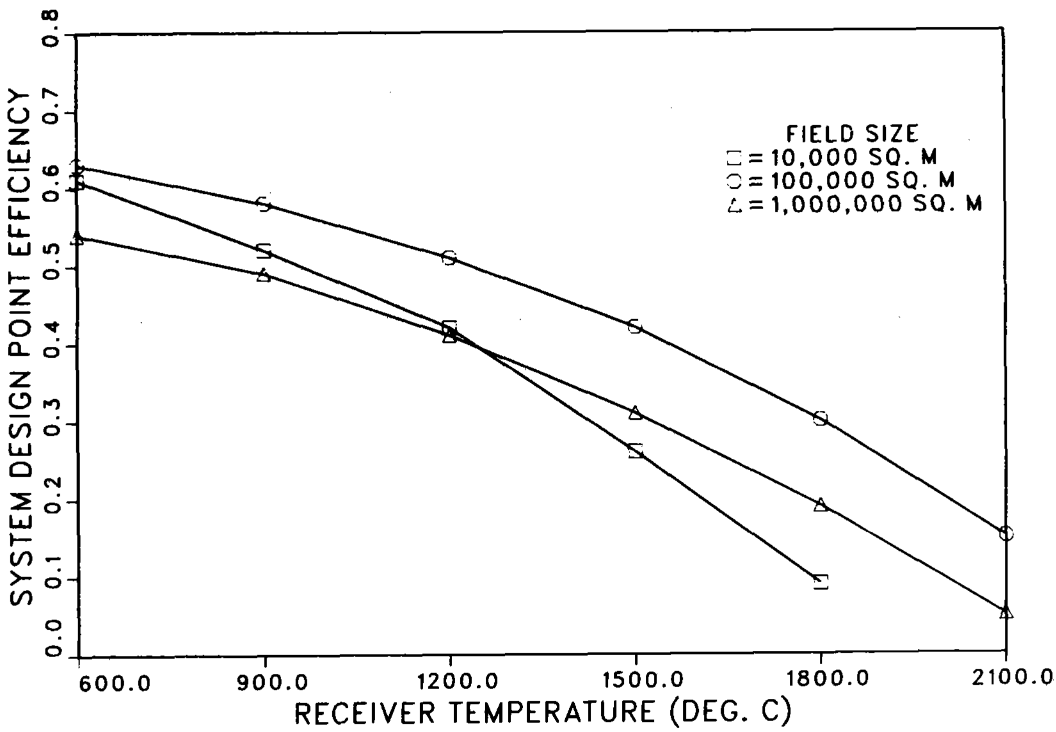

The plot above shows the maximum design point system efficiencies calculated in this study as a function of receiver temperature. All calculations are for simple open-aperture cavity receiver systems and include the effects of inefficiencies in the heliostat field (incidence angle effects, blocking, shadowing, and attenuation), and in the receiver (spillage, convection losses, and reflection and emission losses). Not included are the inefficiencies associated with transferring the energy to a working fluid, or in transporting and storing that working fluid.

THE PERFORMANCE OF HIGH-TEMPERATURE CENTRAL RECEIVER SYSTEMS

Introduction

Background

Solar central receiver technology for the production of electricity has been under development since the mid-1970s. A 10 MWe pilot plant, near Barstow, California, has been operating since April 1982 and continues to demonstrate the technical feasibility, economic potential, and environmental acceptability of the solar central receiver concept. The applicability of the concept to the industrial process heat market has been studied in a number of conceptual design studies funded by the Department of Energy (DOE) and in system-level comparative studies (Ref. 1-3). Current program efforts are being directed toward high-performance systems operating at temperatures much higher than those needed for electricity generation. These high-temperature systems have the potential for achieving high thermodynamic efficiencies in the end-use application and for expanding the applicability of the solar central receiver concept to new applications, including the production of energy-intensive fuels and chemicals.

Purpose of Study

This study is an attempt to understand the effect of thermal and optical limitations on the performance of the solar central receiver system as a function of operating temperature. In a central receiver system, sunlight reflected by a field of computer-driven heliostats (mirrors) is directed toward a receiver on the top of a tall tower. The concentrated sunlight which is intercepted by the receiver and absorbed in the working fluid is then directed to the end-use application. System performance is characterized here by the fraction of the total sunlight which is intercepted by the mirrored surface of the heliostats and ultimately available to be absorbed into the working fluid. The major parameters affecting the system performance are

(1) the density and arrangement of the heliostats,

(2) the size of the heliostats and the amount of canting and focusing in the mirror modules,

(3) the height of the tower and the size and orientation of the heat-absorbing surface, and

(4) the energy losses at the receiver, including principally the convective and radiative (both reflective and emmissive) losses.

Two competing loss mechanisms dominate the performance of the system: spillage loss and receiver thermal losses. The spillage loss is a function of the concentration of the solar flux reaching the receiver and the size and orientation of the receiver aperture. The receiver thermal losses, both radiative and convective, are a function of the receiver temperature, heat absorber area, and aperture area. Because the spillage loss decreases as the aperture area increases, and the receiver thermal losses increase as the aperture area increases, there is a fundamental trade-off which must be investigated to determine the point of maximum performance for a system operating at a given temperature.

In this study, we quantifed these losses and performed this trade-off to determine the maximum efficiency at which a central receiver system can collect high-temperature energy.

Scope and Approach

It seems most probable that future receiver designs, especially those developed for high-temperature applications, will be cavity designs. The large radiative and convective losses which would be sustained by external receivers will probably render them unsuitable for applications at temperatures much higher than currently in use (approximately 600°C). For this reason, we chose to study cavity-type receivers.

A study which attempts to understand the high-temperature capabilities of central receiver systems must do more than simply address the question of what maximum temperature can be reached. The impacts of plant size, collector field size, heliostat size, tower height, and receiver configuration must all be understood. In this study, we have taken a parametric approach towards characterizing the performance of central receiver systems. The range of parameters that we have investigated is shown in Table I. We chose the ranges of these parameters by extending from current technology values in the areas of interest. The extent of the ranges allows trends to be identified.

The approach taken in this study has been to determine the maximum system performance achievable with central receivers at high temperatures, regardless of real-world cost trade-offs. The DELSOL2 (Ref. 4) computer model was used to determine the optimum system configurations based on performance alone. This was accomplished in several steps. First, an initial set of DELSOL2 runs was performed to investigate the importance of the heliostat field parameters, the tower height, and the aperture orientation on the field performance.

A set of nominal receiver geometries, including aperture size, were selected from these initial runs and the receiver radiative losses

TABLE I

STUDY PARAMETERS

Field Size and Configuration	Field Options	Heliostat Size	Receiver Temperature	Peak Flux
10,000 m^2 North Single Cavity	Focus and Cant at a) Single Range b) Slant Range	10 m^2 50 m^2 100 m^2	600°C to 1800°C	.1 MW/m^2 to 1.5 MW/m^2
100,000 m^2 North Single Cavity	Focus and Cant at a) Single Range b) Slant Range Increased Field Density 5 to 20 Percent	10 m^2 50 m^2 100 m^2	600°C to 2100°C	.2 MW/m^2 to 1.5 MW/m^2
1,000,000 m^2 North Single Cavity	Focus and Cant at a) Single Range b) Slant Range	50 m^2 100 m^2	600°C to 2100°C	.2 MW/m^2 to 1.8 MW/m^2
1,000,000 m^2 Surround Multiple Cavity	Focus and Cant at Single Range	50 m^2	600°C to 2100°C	.2 MW/m^2 to 1.8 MW/m^2

(including both reflected and emitted energy) and convective losses were calculated for the range of temperatures and peak fluxes shown in Table I. Finally, the spillage losses were traded off against the receiver thermal losses to arrive at the maximum system performance as a function of receiver temperature and flux levels.

An important relationship exists between flux levels and absorber surface size for high-temperature cavity receivers. Since the receiver thermal losses increase with aperture area, a receiver designer would like to keep the aperture as small as possible. However, the designer is simultaneously constrained to allow as much incoming solar radiation through the aperture as possible. For this reason a single-point heliostat aiming strategy (which produces the tightest possible beam) must be chosen in order to simultaneously minimize the aperture area and maximize the incident radiation.

The implication of this aiming strategy is that, for a given heliostat field size and configuration, the flux levels in the aperture plane are fixed. Thus the only way to change the absorber flux levels while maintaining the same overall power level is to vary the distance between the aperture and the absorber surface. As the absorber surface is moved away from the aperture, the absorber area must be increased in order to fully intercept the solar flux.

For this reason, the values of the peak absorber flux are closely related to both the overall absorber flux levels and the receiver size for a given heliostat field. References to peak absorber flux values should be understood to indicate overall flux levels as well, since these values cannot be varied independently.

Note that the receiver temperature, as used in this study, is not necessarily the same as the working fluid temperature. For the radiative loss calculations, the receiver temperature which is reported is the absorber wall temperature. For the convective loss calculations, the reported temperature represents the average surface temperature inside the cavity. We have not attempted to correlate the receiver surface temperature to a working fluid outlet temperature. Determination of a working fluid temperature is dependent on the heat absorber material properties, the fluid properties, and the fluid velocity, none of which is germane to this study. Similarly, the thermal losses in the transport of the energy to the end-use application, which depend upon the properties of the heat transport fluid, were ignored. Finally, we did not attempt to calculate the receiver conduction losses. These are generally conceded to be small for a well-designed receiver and normally do not represent a driving force in the overall receiver design.

Collector Field Performance

Methodology

In this study, we determined for each selected plant size and receiver temperature the heliostat field configuration and receiver geometry that maximized the receiver-absorbed power. All performance evaluations were based on DELSOL2 calculations of the annual energy collected by the heliostat field. Equinox noon was used as the reference day, and 950 W/m^2 was used as the reference direct normal insolation.

Three plant sizes were chosen to cover the spectrum of central receiver applications: 10,000 m^2, 100,000 m^2, and 1,000,000 m^2. For each plant size, the total number of square meters of reflective surface in the collector field was held constant. This allowed the performance of heliostats having different sizes (or differences in other parameters) to be compared. The 10,000 m^2 field (delivering about 7.5 MW to the aperture plane) is approximately the size of the Central Receiver Test Facility in Albuquerque, New Mexico, and is representative of small remote power or process heat applications. The 100,000 m^2 field (delivering about 75 MW to the aperture plane) is slightly larger than the 10 MWe pilot plant in Barstow and is representative of commercial process heat or fuels and chemicals applications. The 1,000,000 m^2 field (delivering about 670 MW to the aperture plane) is approximately the size proposed for commercial central receiver electricity-generating plants.

An initial set of DELSOL2 runs was performed to establish the basic geometry of the collector field, tower, and aperture orientation. These runs were performed with the assumption that there were no radiation or convection losses from the receiver. The following paragraphs will discuss the parameters which were varied, and the results of these runs.

Heliostat Size

Heliostat sizes were chosen to represent the current second-generation size (50 m^2) and the extrapolation of this design to a larger mirror area (100 m^2); a very small heliostat size (10 m^2) was also studied to characterize any potential performance gain for small plant sizes. Mirror reflectivity for all sizes was 0.89, and tracking and surface error distributions were assumed to be identical for all sizes. Mirror panels were focused in two directions and canted on-axis. The default heliostat geometry in DELSOL2, with 12 cant panels in a 2x6 array, was used for each size.

Aperture Orientation

The orientation of the aperture (defined here as the angle of the aperture plane with respect to the vertical) was varied in six increments from 0 degrees (vertical) to 75 degrees (nearly horizontal) for the small field size, and to 50 degrees for the larger field sizes. For each aperture orientation, DELSOL2 determined the tower height and the heliostat field configuration which maximized the field efficiency.

Because of its effect on the aperture vertical height, the aperture orientation has an effect on the receiver convective losses. Reducing the vertical height of the aperture reduces the convective loss. For this reason, one would like to keep the aperture as nearly horizontal as possible, while keeping the spillage losses at an acceptable level.

Focus and Cant Strategies

Every heliostat in this study is composed of 12 mirror modules. The terms focusing and canting mean, respectively, focusing (curving) the individual mirror modules and tilting them slightly with respect to the plane of the heliostat. Each technique produces a tighter and less divergent beam at the aperture. We investigated the impact of several focusing and canting strategies on all of the field and heliostat sizes. We also examined the effect of focusing as opposed to canting.

Heliostat Field Density

The field density refers to the total reflective area per unit area of land. Field density is typically not a constant throughout the field, but decreases with distance from the tower. If the density at a particular radius is too high, the heliostats tend to be shadowed or blocked by their immediate neighbors. If the field density is too low, the field becomes overly large and the mean radius to the tower becomes larger, causing larger beam divergence and atmospheric attenuation. The nominal field densities used in this study were determined with a correlation developed by the University of Houston and incorporated in DELSOL2. Variations were made in several increments on either side of these nominal values to determine whether improvements could be obtained. In every case analyzed, the performance decreased for any density but the nominal values.

Results

Total field efficiency as a function of aperture orientation is shown in Figures 1 and 2. The total field efficiency accounts for losses due to cosine (incident angle) effects, shadowing and blocking, atmospheric attenuation, and spillage. The nominal aperture size was chosen to give a

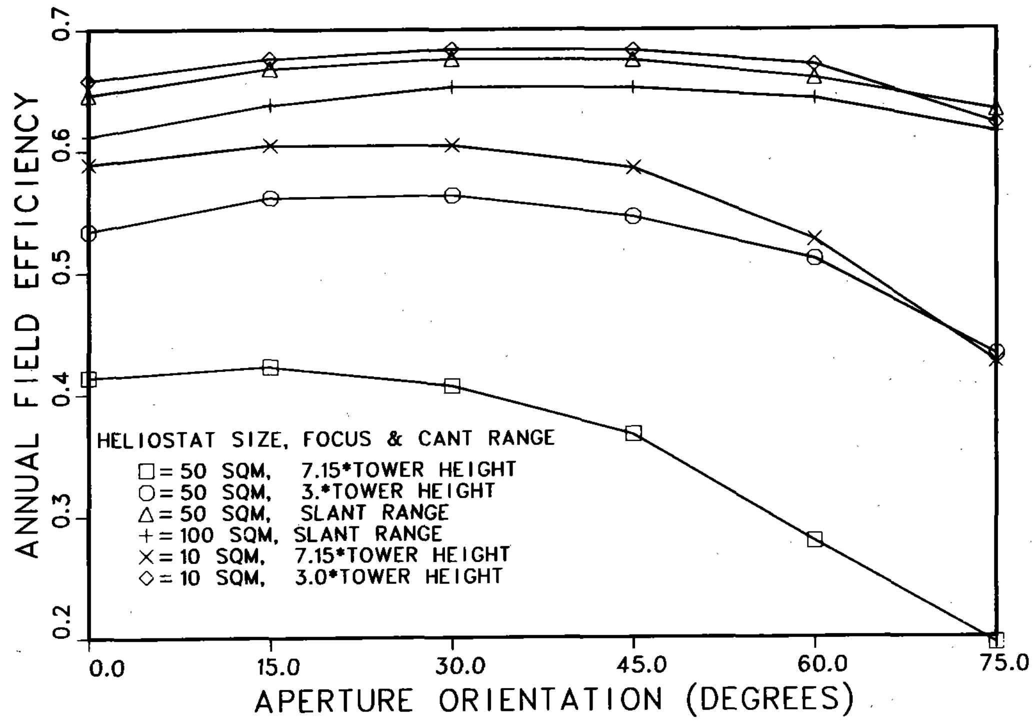

Figure 1. Field Efficiency Versus Aperture Orientation for the 10,000 m^2 Field Size

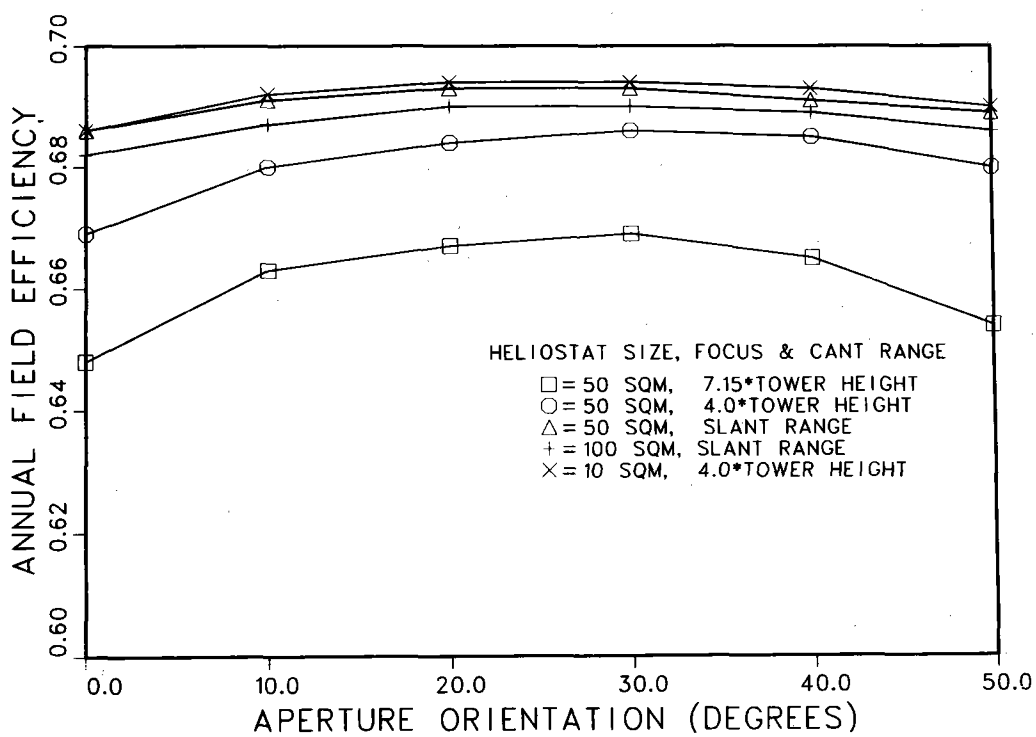

Figure 2. Field Efficiency Versus Aperture Orientation for the 100,000 m^2 Field Size

receiver spillage (the fraction of the radiation incident on the aperture plane which does not pass through the aperture) of about 10 percent. This nominal aperture size was then held constant as aperture orientation was changed. A single aim point was used to minimize the receiver spillage, and an elliptical aperture shape was used to minimize the aperture area.

Figure 1 is a plot of field efficiency versus aperture orientation for the 10,000 m^2 size field. At this relatively small field size, the optimum single focus and cant range for the entire heliostat field is about 3 tower heights. This range provides a significant increase in field performance over the DELSOL2 default value of 7.15 tower heights. Focusing and canting each heliostat at its slant range increase the field performance by about 10 percent (0.56 to 0.67).

Increasing the heliostat size from 50 m^2 to 100 m^2 decreases the field efficiency by only 2 percent (0.67 to 0.65). Decreasing the heliostat size to 10 m^2 and using the optimum single focus and cant range increases the field efficiency by only 1.5 percent (0.67 to 0.68).

Note that the field efficiency is relatively insensitive to the aperture orientation for angles between 15 and 30 degrees for single focus and cant fields, and for angles between 15 and 45 degrees for fields focused and canted at the slant range. The greater range of angles for fields focused and canted at the slant range occurs because the tower height can be increased without a significant decrease in performance.

The field efficiency curves for the 100,000 m^2 field are shown in Figure 2. The trends are similar to those identified for the 10,000 m^2 field. However, the impacts of changing the heliostat size and the focus and cant strategy are less pronounced. The gain in field performance as a result of focusing and canting heliostats at the slant range--as opposed to a single focus and cant range--is about 1 percent. The changes in the field efficiency caused by increasing or decreasing the heliostat size are less than 1 percent.

The impact of the aperture orientation for the 1,000,000 m^2 field size is not shown here, since it is very similar to that found for the 100,000 m^2 field sizes. Changing the heliostat size and the focus and cant strategy at the 1,000,000 m^2 field size has almost no effect on the field performance.

Total field efficiency is plotted as a function of tower height in Figures 3, 4, and 5 for the 10,000 m^2, 100,000 m^2, and 1,000,000 m^2 fields, respectively. Figure 3a, which characterizes the impact of focus and cant strategies, shows that the increases gained by focusing and canting the field at the slant range are caused almost entirely by the canting. Figure 3b shows the impact of heliostat size on field performance.

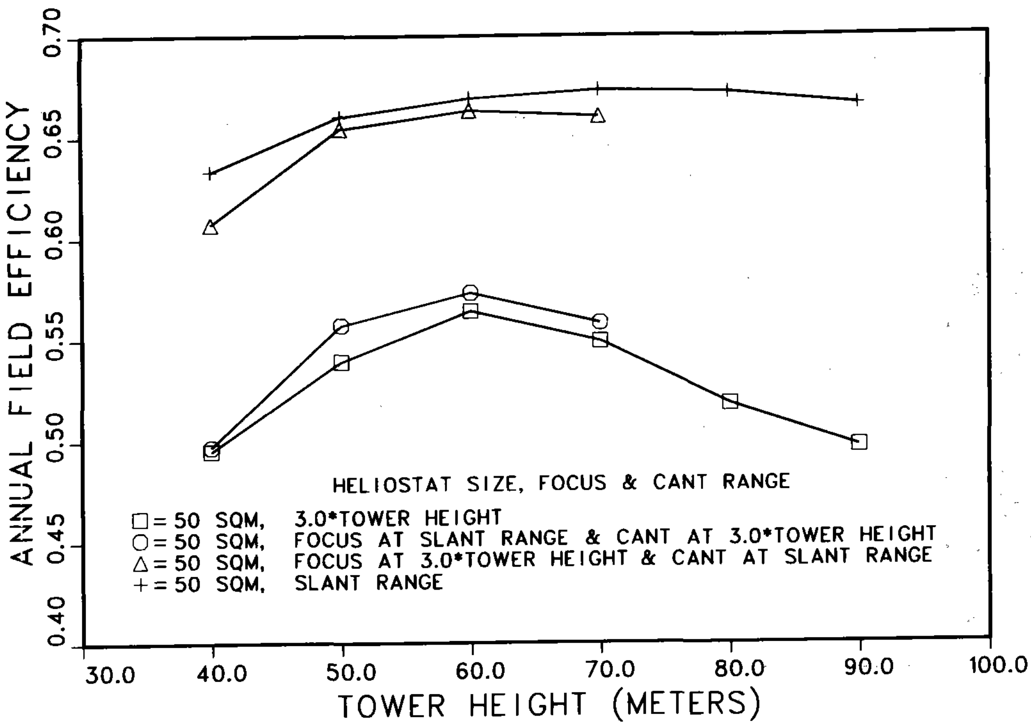

(a) Effect of Focus and Cant Strategies

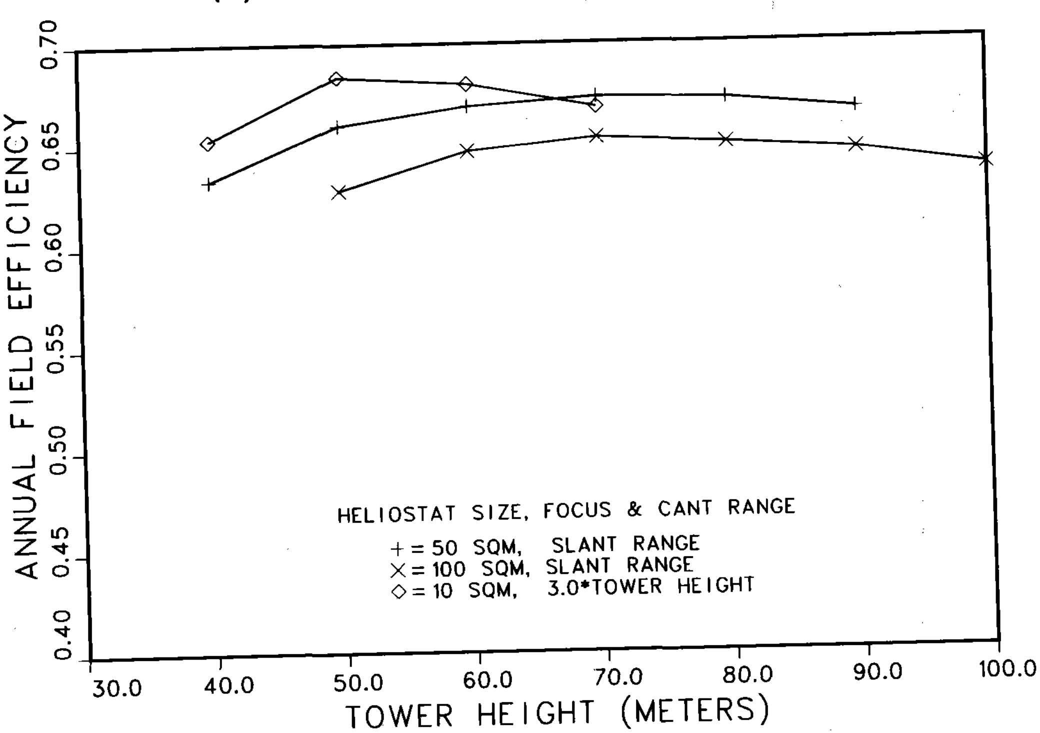

(b) Effect of Heliostat Size

Figure 3. Field Efficiency Versus Tower Height for the 10,000 m^2 Field Size

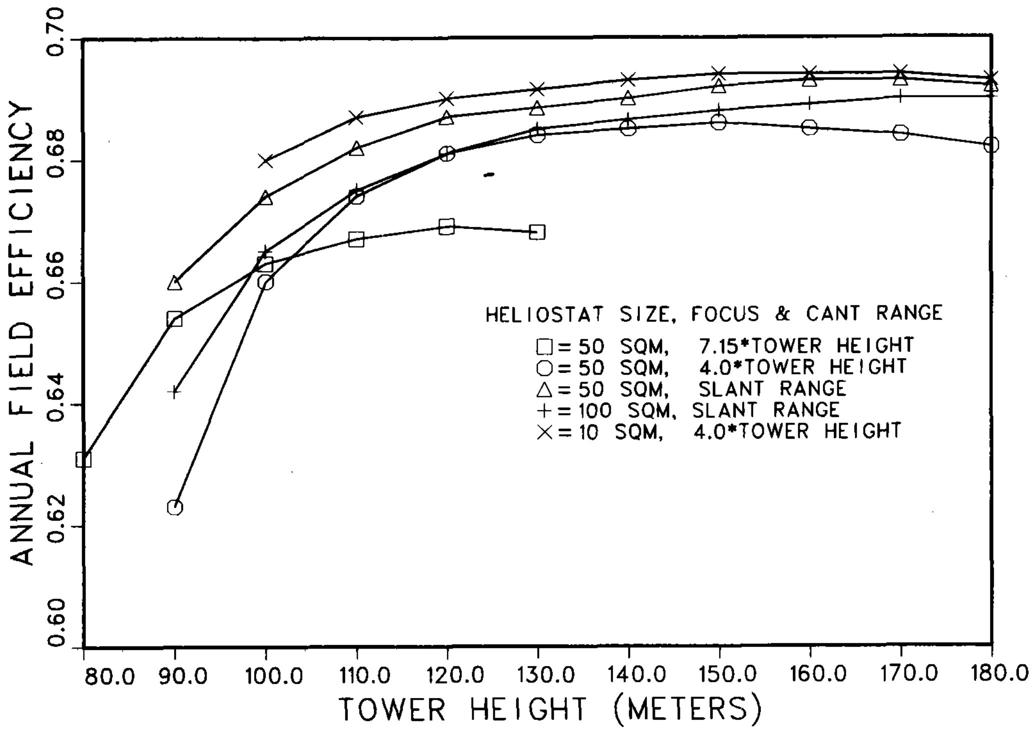

Figure 4. Field Efficiency Versus Tower Height for the 100,000 m^2 Field Size

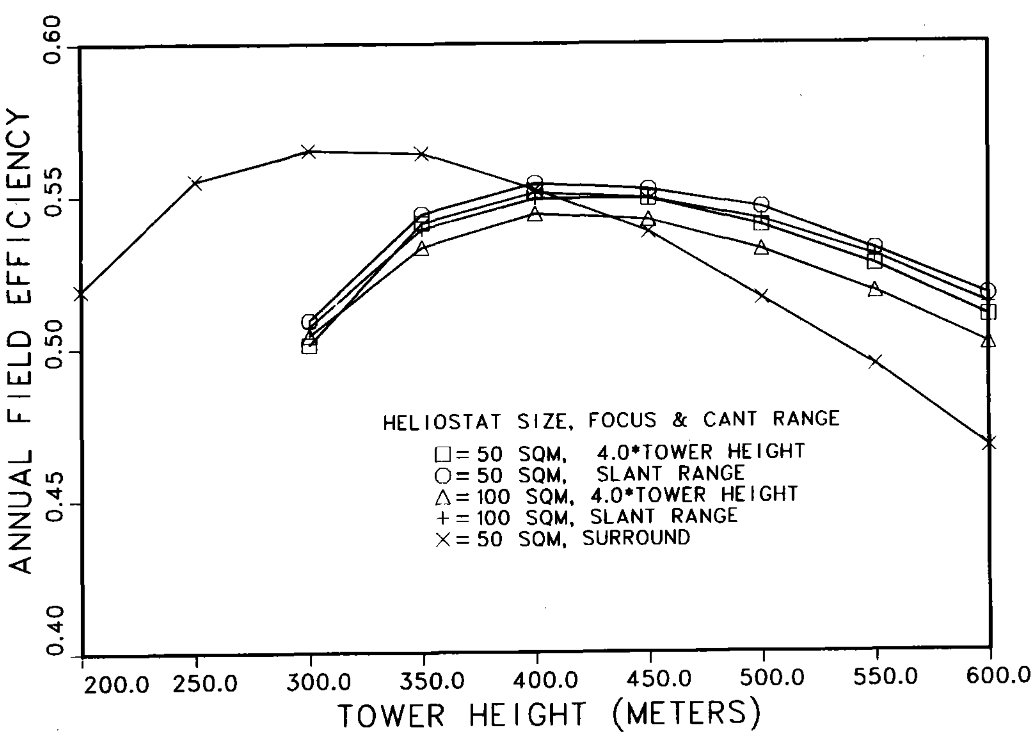

Figure 5. Field Efficiency Versus Tower Height for the 1,000,000 m^2 Field Size

An interesting interaction occurs between the focus and cant range, the tower height, and the mean field radius. For a given receiver and field size, a heliostat field with a single, fixed focus and cant range will tend to have a longer mean field radius and a shorter tower; choosing a single focus and cant distance effectively determines the heliostat slant range that will minimize spillage. If negligible variations in the field density are assumed, then a given field size requires a fixed area of land. As the mean radius from the tower increases, the arc length within the aperture acceptance angle increases. Thus, the required land area can be constructed in a wider and narrower strip, allowing more of the heliostats to be positioned closer to the chosen focus and cant distance. Because, in fact, the heliostat spacing increases with increasing field radius, there is less shadowing and blocking, and shorter towers reduce cosine and attenuation losses.

Conversely, when the heliostats are focused and canted at their individual slant ranges, the trend is toward a compact field which is clustered very close to the base of the tower to minimize the spillage and attenuation losses. This configuration tends to demand fairly tall towers, so that the cosine and shadowing and blocking losses can be reduced.

As the heliostat field size becomes larger, the land area required forces the field away from the base of the tower, and the effect of focusing and canting becomes smaller. In fact, the results of varying the focusing and canting strategy indicate that for fields 100,000 m^2 and larger, a single focus and cant range for all heliostats is nearly as good as focusing and canting each heliostat at its slant range. The optimum focus and cant range for the north field configurations studied is between 3 and 4 tower heights.

For fields focused and canted at the slant range, there is a broad maximum to the field efficiency with respect to the tower height. This is important to the system designer, because in an actual plant design the cost of the tower has to be traded off against the performance and cost of the heliostat field. Thus, the plant cost can be reduced by using a shorter-than-optimum tower without a significant reduction in the field performance.

In addition to these north field configurations, two surround field configurations were studied. A surround-field, four-receiver configuration with a receiver oriented on each of the cardinal compass points was investigated for the largest field size. Figure 5 shows that this configuration leads to a shorter tower and a slight increase (2 percent) in field performance.

At the 100,000 m^2 field size, a surround-field with a single downward-facing aperture was found to result in a much taller optimum tower height (240 m versus 160 m for 50 m^2 heliostats focused and canted at the slant range) and a slight decrease (3 percent) in the field performance.

Receiver Geometry

The basic receiver geometry used for this study is shown in Figure 6. The heat-absorbing surface is a section of a right circular cylinder with a radius centered at the center of the aperture. The bottom surface of the receiver is horizontal and at the level of the bottom of the aperture. The height of the heat-absorbing surface is determined by DELSOL2 according to the geometry dictated by the minimum field radius, the tower height, and the aperture height and orientation. On the basis of the flux maps produced by DELSOL2, the included angle of the absorber surface was varied from a minimum of 120 degrees to a maximum of 160 degrees.

Although not perfect for all possible combinations of absorber surface radius and included angle, this design generally provided an adequate generic representation of future high-temperature cavity receiver designs. This is particularly true as the area of the aperture gets smaller relative to the interior surface area, because the situation approaches that of a Hohlraum cavity and the exact configuration of the surfaces behind the aperture becomes increasingly less important in determining the radiative losses. Furthermore, given the necessity of using a single-point aiming strategy, this receiver geometry tends to produces more uniform fluxes on the heat-absorbing surface than, for example, a plane surface. Peak-to-average flux values ranged from 3.3 for the receivers with the lowest peak absorber fluxes to 2.0 for the highest peak flux receivers.

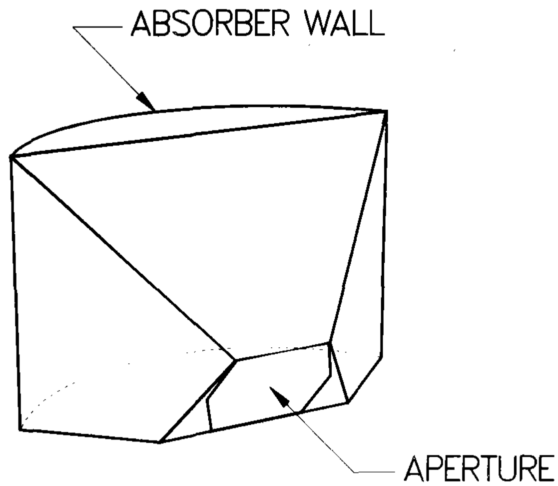

Figure 6. Cavity Receiver Isometric View

The receiver geometries which were analyzed are listed, along with the values for associated peak absorber flux and power incident on the aperture, in Table II.

Radiation Loss Model

The receiver radiative and convective losses were handled independently. The radiative losses were calculated by the computer program RADSOLVER (Ref. 5) on the basis of three sets of data: a description of the geometry of the cavity, the distribution of the incoming solar flux on the interior surface, and the surface reflectivity data.

The geometrical description comes in the form of the shape (or view factors) calculated by SHAPEFACTOR (Ref. 6). SHAPEFACTOR is a fairly general computer code for finding the view factors between any set of 3- or 4-sided planar surfaces. Thus, the interior surfaces of the cavity had to be made planar in order to calculate the view factors. To do this, the curved cylindrical heat-absorbing surface was approximated as a portion of a right polygonal cylinder. The elliptical aperture was approximated by a combination of a square and two triangles, which produced the aperture shape shown in Figure 6. The size of the square was chosen to minimize the difference between the total area of the approximation and the area of the ellipse.

An expanded layout of the receiver interior surfaces is shown in Figure 7. The absorber surface, which is assumed to have a gray body reflectance of 0.1, occupies an included angle of nominally 120 degrees centered on due south. The other surfaces in the receiver are assumed to be made of a refractory material with a gray body reflectivity of 0.4.

The description of the incoming solar radiation is in the form of flux maps generated by DELSOL2, which calculates the point flux values for a matrix of points on the absorber surface. These point values had to be integrated and averaged over each of the zones in order to be used in the radiation model. Figure 8 shows examples of flux maps for both the point values and the integrated and averaged values. Note from Figure 7 that the heat-absorbing surface was divided into twenty zones (four azimuthally and five vertically). Because the flux varies quite sharply in the vertical direction, the adequacy of this grid was checked for a few selected cases by increasing the number of vertical zones to 10. The radiative losses for the forty zone runs were almost identical to the twenty zone runs.

With the SHAPEFACTOR data, surface reflective properties, and averaged solar radiation values, RADSOLVER calculates the radiation exchanges between the various surfaces to arrive at the net radiative exchange with the environment and the temperature of the inactive surfaces. Although RADSOLVER is capable of performing the radiation analysis on an arbitrary number of wavelength bands, a single-band (gray body) analysis was used for the results presented in this report.

TABLE II

RECEIVER GEOMETRIES

Field Parameters		Aperture Size and Orientation	Radius (m)	Included Angle [a]	Height (m)	Peak Absorber Flux (MW/m^2)	Incident Design Point Power (MW) [b]
Size:	10,000 m^2	3.2 x 2.8 m	11.5	120	9.7	.10	7.70
Annual Efficiency:	0.72[b]	30°	5.75	120	5.5	.25	
Tower Height:	70		4.0	120	4.2	.45	
			3.0	150	3.5	.70	
			1.6	135	2.5	1.40	
Size:	100,000 m^2	8.5 x 7.0 m	25.0	120	23.9	.20	76.1
Annual Efficiency:	0.70[b]	30°	20.0	120	20.3	.27	
Tower Height:	160		15.0	120	16.7	.40	
			11.5	120	14.2	.56	
			7.5	150	11.3	1.00	
			5.0	140	9.5	1.50	
Size:	1,000,000 m^2	22.5 x 18.0 m	60.0	120	59.5	.24	672.0
Annual Efficiency:	0.64[b]	30°	50.0	120	52.4	.30	
Tower Height:	450		40.0	120	45.4	.43	
			30.0	120	38.3	.62	
			20.0	120	31.3	1.05	
			12.5	120	26.0	1.82	

[a] The included angle of the heat absorbing surface.

[b] The annual field efficiency and the design point power reported in this table represent the 50 m^2 heliostat size, focused and canted at the slant range, and excludes spillage losses.

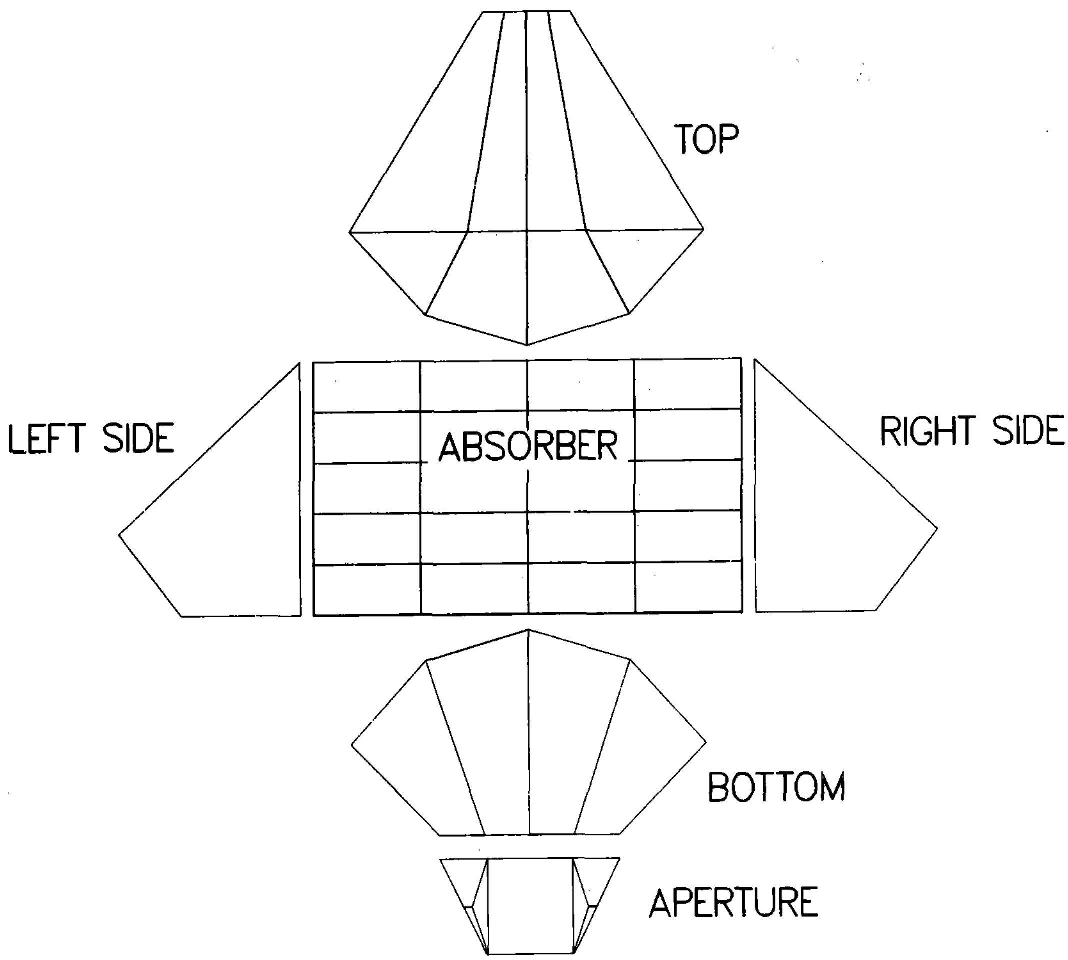

Figure 7. Expanded Layout of Cavity Geometry

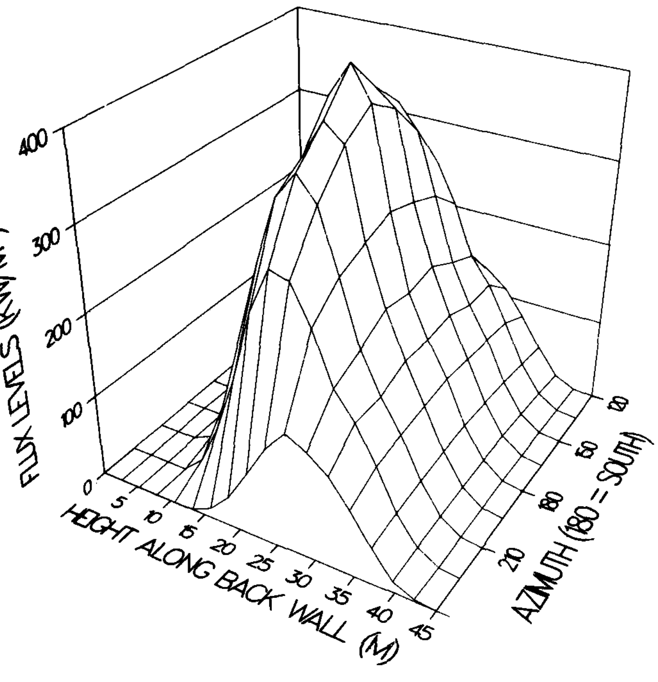

(a) Point Flux Distribution

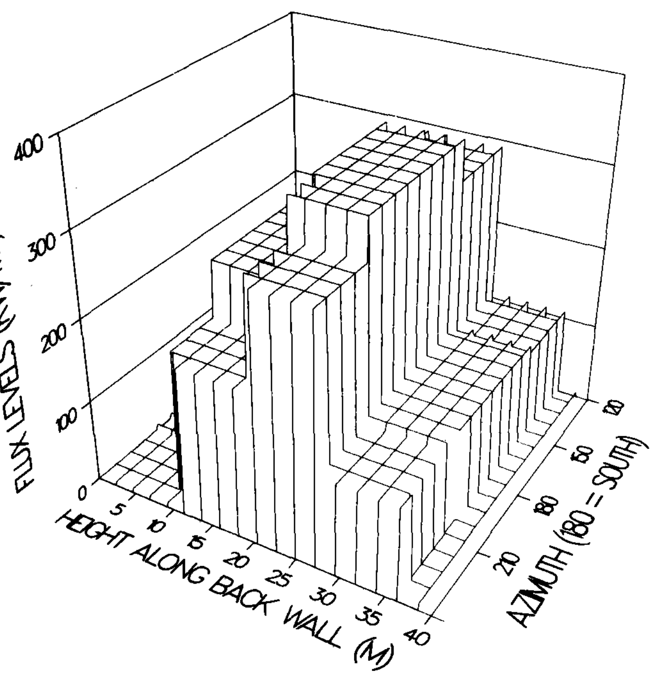

(b) Averaged Flux Distribution

Figure 8. Example of Solar Flux Distributions

Receiver Radiative Loss Fractions

The receiver radiative loss fraction is the fraction of the energy incident on the receiver interior surfaces which is lost because of reradiation and reflection out of the aperture. Figures 9, 10, and 11 show plots of the radiation loss fraction for various receiver temperatures as a function of the peak flux on the heat-absorbing surface. The receiver temperature is the heat-absorber surface temperature as specified in the RADSOLVER model. The temperature was assumed to be uniform over the entire heat-absorbing surface. (Sensitivity to this assumption was checked by running several cases in which there was a 100^{o}C temperature gradient from bottom to top of the heat-absorbing surface. This had a negligible effect on the radiative loss fraction.) The temperature of the non-heat-absorbing surfaces was calculated by RADSOLVER under the assumption that these surfaces were adiabatic.

Inspection of Figures 9, 10, and 11 shows that the radiative loss fractions for a given heliostat field, aperture size, and receiver temperature do not undergo much change over the range of peak absorber

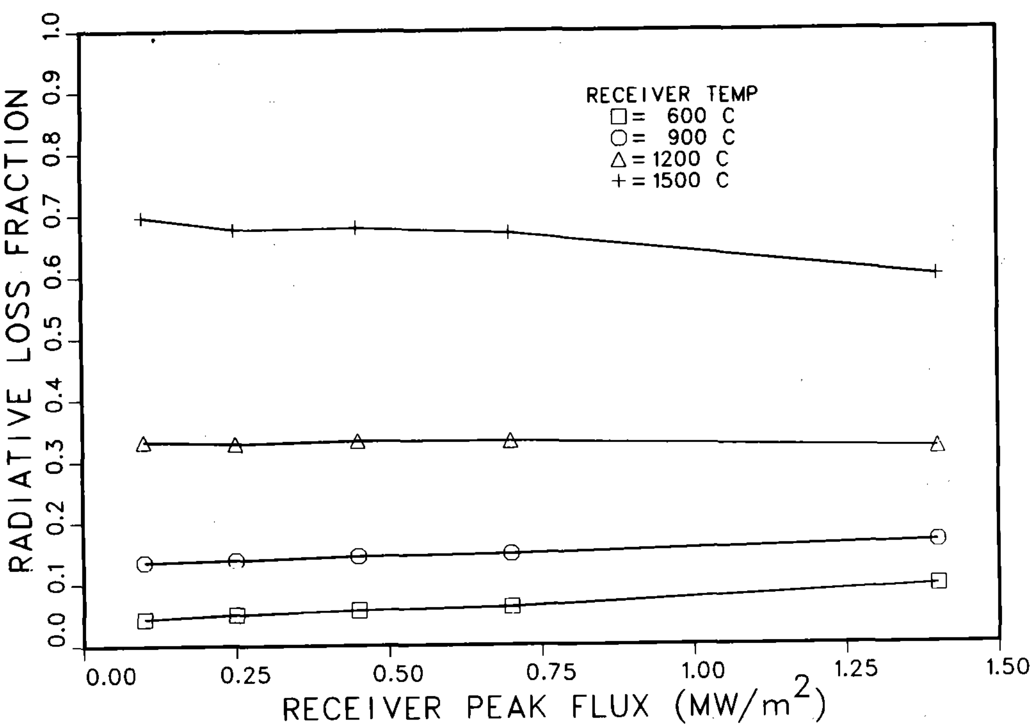

Figure 9. Radiative Loss Fractions for a 10,000 m^2 Field

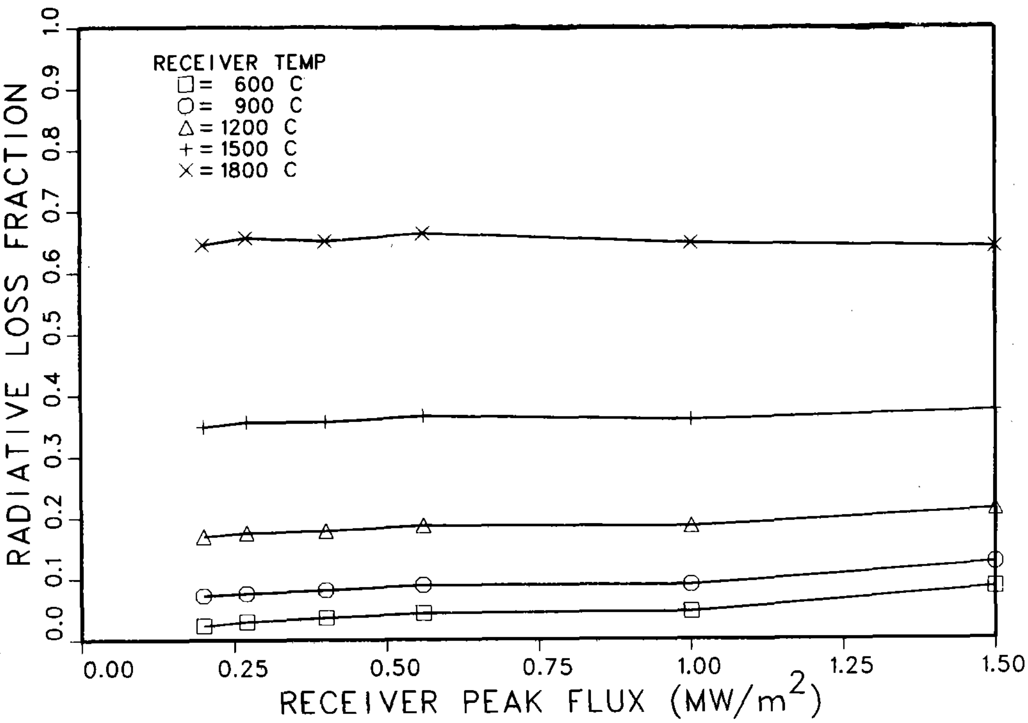

Figure 10. Radiative Loss Fractions for a 100,000 m^2 Field

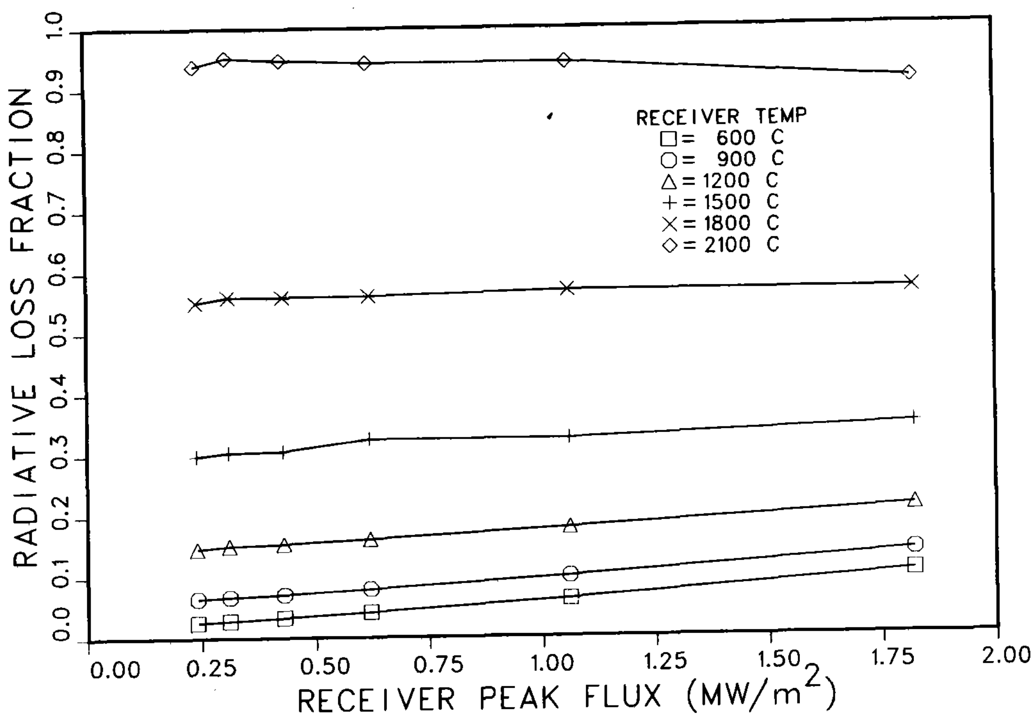

Figure 11. Radiative Loss Fractions for a 1,000,000 m^2 Field

flux. At the lower temperatures, the loss fraction increases slightly with increasing receiver peak flux; this results from the increase in the view factor of the interior surfaces as the receiver size is decreased. At the highest temperatures, the loss fraction decreases slightly with increasing receiver peak flux; this unexpected result is caused by a relative decrease in the amount of energy lost from the non-heat-absorbing side walls.

For low peak flux receivers, the energy falling on the heat-absorbing surface outside of an absorber surface included angle of 120 degrees is negligible. This small amount of energy is easily distributed along the receiver side walls. As the receiver peak flux is increased (i.e., receiver size is decreased), the flux levels on the side walls increase to rather large values. Therefore, the absorber surface included angle was increased for the high peak flux receivers to as much as 160 degrees. This improved the high flux performance in two ways: first, it decreased the flux levels on the refractory surfaces, and, second, it decreased the view factor from the side walls to the environment.

Thus, at the highest temperatures, where the energy lost from the side walls is most significant, the decrease in the side-wall view factor causes the receiver radiative loss fraction to decrease slightly. At the low flux levels, the change in included angle made negligible difference in the radiative performance, since the flux incident on the side walls was quite low. The resulting receiver included angles are listed in Table II. When the receiver radiative losses at the larger included angle were similar to those losses at the 120^{0} included angle, the smaller angle was used.

Convective Loss Model

Predicting natural convection losses from cavity receivers is a complicated task requiring additional study. The recent correlation developed by Kraabel (Ref. 7) provides the most appropriate tool to date. This correlation is based on a large cavity experiment (2.2 m cube) and two smaller cubical cavity experiments of 0.2 m and 0.6 m. Comparison of these experimental results indicates that the heat transfer coefficient for open cavities is independent of cavity size. The correlation is therefore believed to be applicable to larger cavities. (See Appendix A.)

The natural convection heat transfer occurs as a turbulent boundary layer process, principally on the surfaces below the top of the aperture. The correlation for the heat transfer coefficient is:

$$h = 0.81 * (T_w-T_a)^{0.43} * (A_{bot}/A_{tot})^{0.63} \qquad (1)$$

where: h is the convective heat transfer coefficient (W/m^2 - ^{o}C)
T_w is the receiver wall temperature (^{o}C)
T_a is the ambient temperature (^{o}C)
A_{bot} is the interior area of the receiver below the top of the

aperture (including the bottom surface) (m^2)

A_{tot} is the total interior area of the receiver (all sides plus top and bottom surfaces) (m^2)

and the fluid properties are evaluated at the ambient air temperature.

The heat transfer from the cavity is then

$$Q = h * A_{tot} * (T_w - T_a) \qquad (2)$$

Examination of Equations (1) and (2) shows that with this model the convective loss is proportional to the terms

$$(T_w - T_a)^{1.43} * A_{tot}^{0.37} * A_{bot}^{0.63}$$

This expression emphasizes the strong dependence of the model on the receiver wall temperature. The dependence of the convective losses on the geometry of the receiver and the aperture orientation can be seen in their impact on the terms A_{tot} and A_{bot}.

Note that all of the internal surfaces of the cavity are considered to be active convective heat transfer surfaces. The non-heat-absorbing surfaces typically receive enough reflected and reradiated energy to become as hot or hotter than the heat-absorbing surfaces. The convection from these surfaces is included in the overall receiver loss because the source of this energy is the solar flux incident upon the receiver.

Receiver Convective Loss Fractions

The receiver convective loss fraction is the fraction of the energy incident on the receiver which is lost as the result of convection. Figures 12, 13, and 14 are plots of the convective loss fraction for various receiver temperatures as a function of the receiver peak flux. Each plot was generated using the convective loss correlation from Equation 1 on the receiver geometries determined from DELSOL2. The peak receiver flux for each geometry was also determined using DELSOL2.

The convective loss fractions increase geometrically as the receiver peak flux decreases (i.e., as the receiver size increases). This is a direct result of the relationships intrinsic in the form convective loss correlation. As shown above, for a given temperature the heat loss is proportional to

$$A_{tot}^{0.37} * A_{bot}^{0.63}$$

A_{tot} is roughly proportional to the receiver radius squared while A_{bot} is roughly proportional to the receiver radius. Thus the convective loss is proportional to the receiver radius to about the 1.4

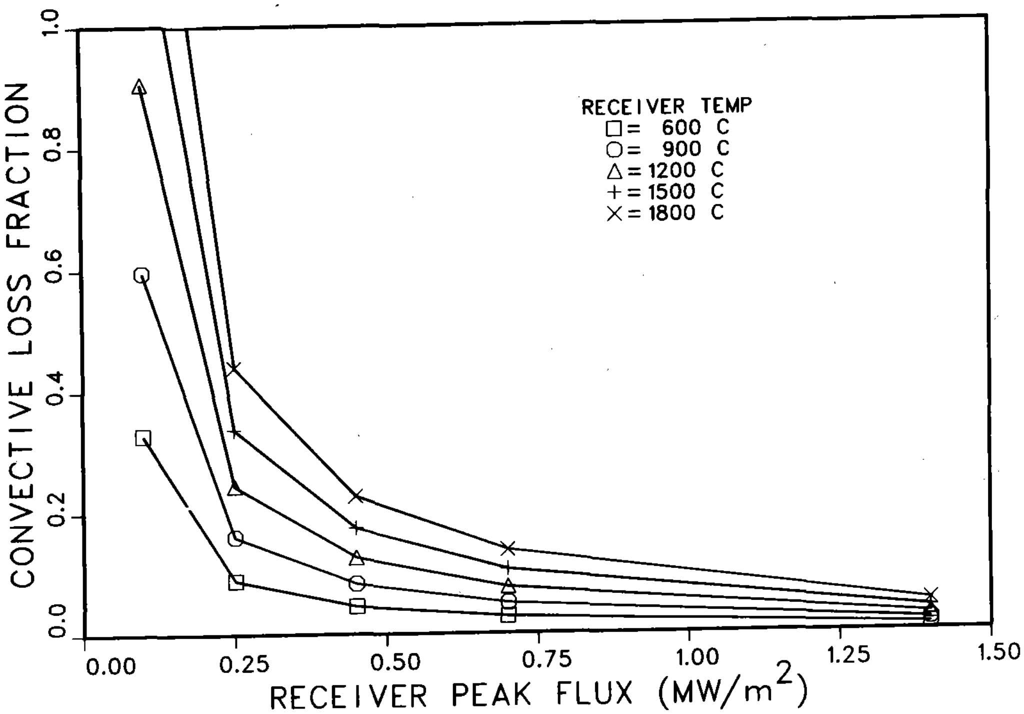

Figure 12. Convective Loss Fractions for a 10,000 m^2 Field

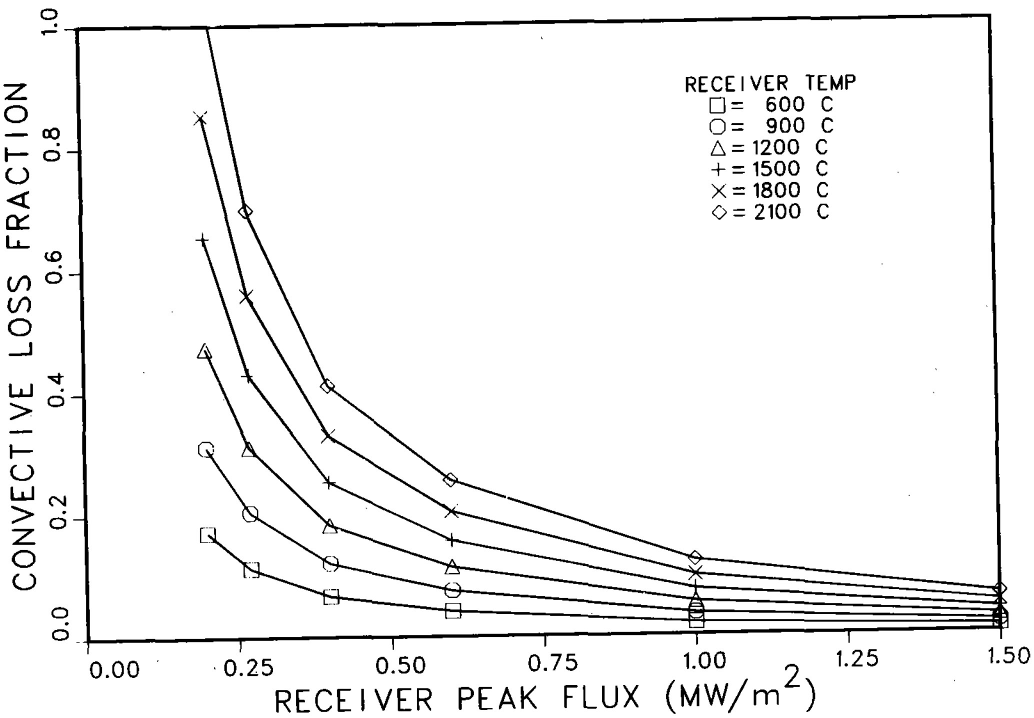

Figure 13. Convective Loss Fractions for a 100,00 m^2 Field

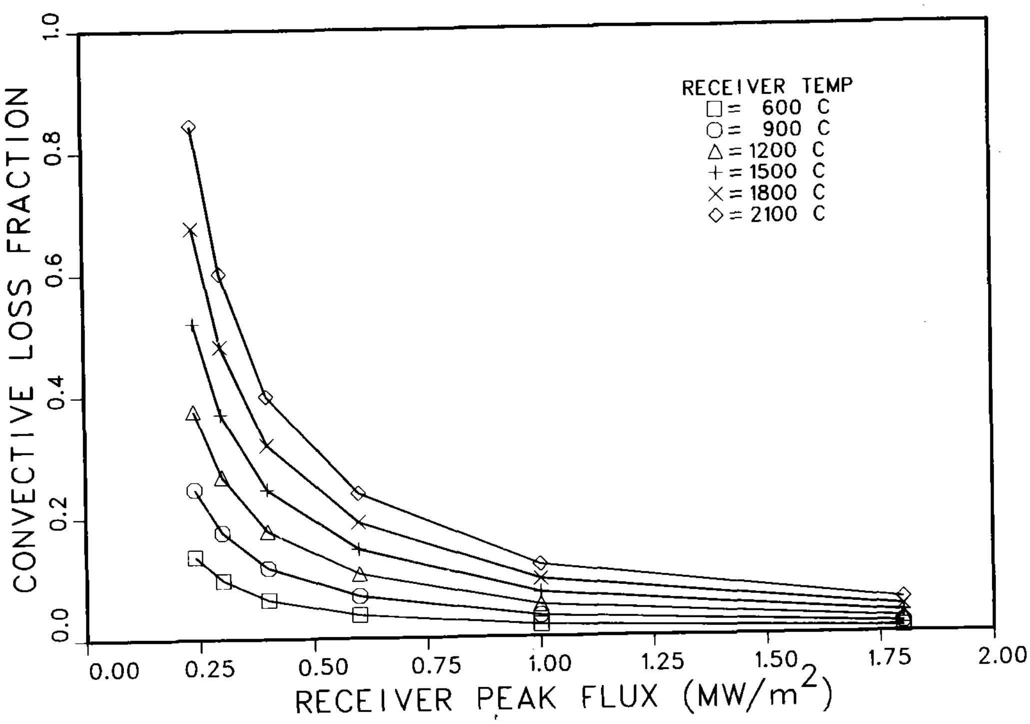

Figure 14. Convective Loss Fractions for a 1,000,000 m^2 Field

power. Because the peak flux varies inversely with the receiver radius, the convective heat loss varies with the peak flux to the -1.4 power. This relationship is demonstrated in the shape of the curves shown in Figures 12, 13, and 14.

Convective Loss Sensitivity

Because the convective heat loss is sensitive to the total receiver interior area, it may be possible in some cases to improve the system performance by reducing the receiver height and, therefore, the convective loss fraction. The height of the absorber surface is determined by the minimum field radius, the tower height, and the aperture height. If, for example, the minimum field radius is increased, then the heat-absorbing surface height is reduced. This reduces the convective loss, but only at the cost of decreasing the field performance. Figure 15 plots the approximate relative change in the receiver efficiency that results from changes in the receiver height. This potential improvement in the receiver performance must then be weighed against the change in the field performance.

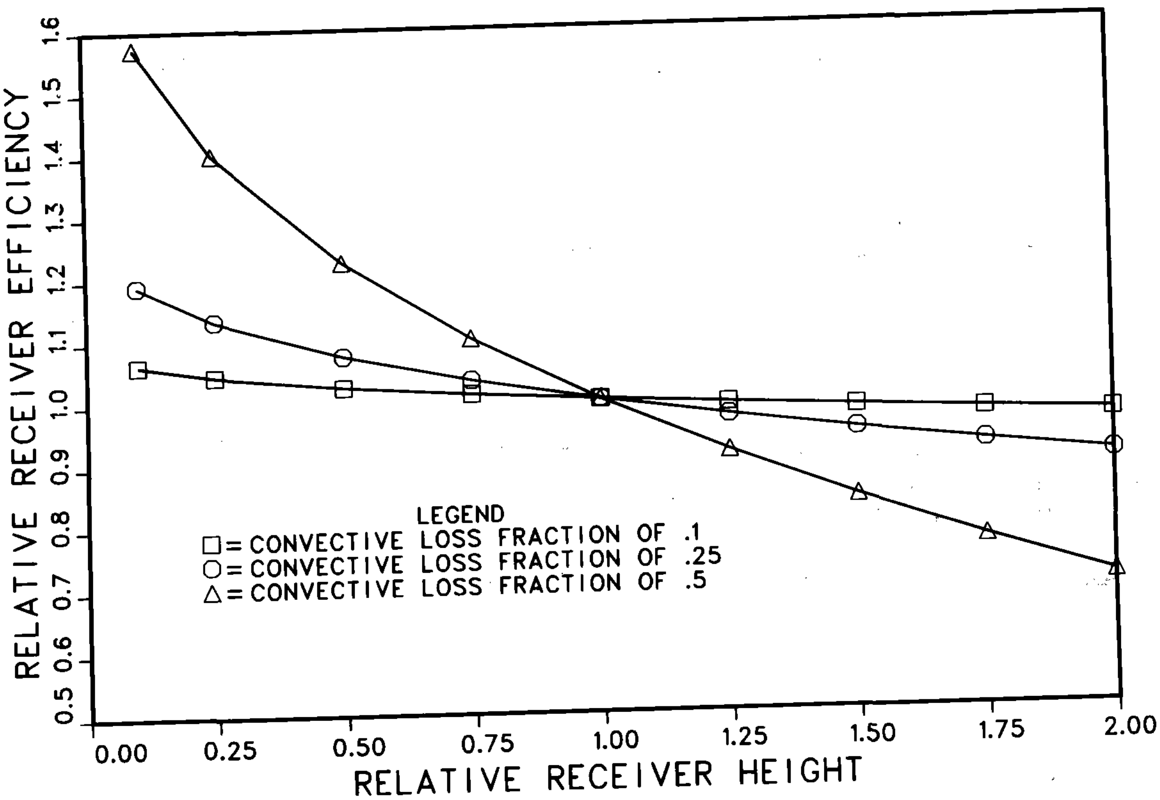

Figure 15. Sensitivity of Receiver Convective Loss Fraction to Changes in Receiver Height

Table III illustrates the effect of minimum field radius on the receiver height and the field performance for the 10,000 m^2 field size using 50 m^2 heliostats focused and canted at the slant range. The initial increase in the minimum field radius (0.75 to 1.5 tower heights) results in a slight decrease in field performance and a large decrease in receiver height. Subsequent increases in the minimum field radius produce more significant decreases in the field performance for slight decreases in the receiver height. This relationship also holds for the larger field sizes. Therefore, a minimum field radius of 1.5 tower heights was used in the determination of the receiver geometries.

TABLE III

MINIMUM FIELD RADIUS EFFECT ON FIELD EFFICIENCY

Minimum Field Radius as a Multiple of the Tower Height	Field Efficiency	Receiver Height
.75	.67	10.0 m
1.5	.64	5.5 m
2.5	.54	4.1 m
3.5	.42	3.6 m
5.0	.16	3.0 m

System Performance

Receiver Losses

The receiver thermal losses presented in the previous section were calculated using the nominal aperture areas determined during the heliostat field optimizations. The final trade-off between the receiver thermal losses and the spillage loss was performed in the following manner.

For each field size, the spillage was determined for a range of aperture sizes, typically ± 30 percent of the nominal size. The receiver radiative loss fraction was assumed to be proportional to the aperture area. This is a good assumption because, for small changes in the aperture area, the view factor between the interior of the cavity and the aperture does not change significantly. The receiver convective loss fraction was assumed to be proportional to the vertical aperture height raised to the 0.63 power, in accordance with the convective loss model. This proportionality holds as long as the receiver radius remains constant. These relationships were used to determine the minimum receiver loss fraction within the selected range of aperture sizes.

Tables IV, V, and VI list the optimized aperture sizes and receiver loss fractions for three selected absorber peak fluxes for the 10,000 m^2, 100,000 m^2, and 1,000,000 m^2 fields, respectively. Note that for a given temperature, the optimized aperture sizes are roughly independent of the peak absorber flux. The radiative loss fractions also do not vary significantly with the peak flux. The major variation in the receiver loss fraction is due to the convective losses. Because of the large receiver areas (see Table II) that are required to keep the peak flux levels low, the convective losses contribute significantly to the total receiver loss fraction. At the highest peak fluxes, where the receiver size is relatively small, the convective losses are much less significant.

Table VII lists receiver loss fractions for a receiver temperature of 1200°C. This table also shows the importance of the convective losses at low peak flux levels. Note, however, that receiver loss fractions for a 100,000 m^2 field are smaller than those for either a 10,000 m^2 or a 1,000,000 m^2 field. This smaller fraction is caused by both slightly smaller spillage losses and by smaller radiative losses. The lower spillage loss is the result of the higher concentration ratio achievable at the 100,000 m^2 field size, while the lower radiative losses result from the fact that receivers at this field size have the lowest ratio of aperture area to absorber area.

System Efficiencies

In this study, total system efficiency represents the effectiveness of the system in converting sunlight to thermal energy

TABLE IV. RECEIVER LOSS FRACTIONS FOR A 10,000 m^2 FIELD

Absorber Peak Flux (MW/m^2)	Receiver Temp (°C)	Aperture Size (m) W X H	Spillage Loss Fraction	Convective Loss Fraction	Radiative Loss Fraction	Total Receiver Loss Fraction
	600	4.0 x 3.5	.03	.10	.08	.21
	900	3.5 x 3.0	.06	.17	.17	.39
.25	1200	3.0 x 2.6	.12	.23	.29	.64
	1500	2.5 x 2.2	.23	.29	.41	.93
	1800	0.5 x 0.44	.85	.14	.03	(1.01)
	600	4.0 x 3.5	.03	.03	.10	.16
	900	3.5 x 3.0	.06	.05	.17	.29
.70	1200	3.0 x 2.6	.12	.07	.29	.48
	1500	2.5 x 2.2	.23	.09	.41	.73
	1800	0.5 x 0.44	.85	.04	.03	.92
	600	3.5 x 3.0	.06	.01	.11	.18
	900	3.5 x 3.0	.06	.02	.20	.27
1.4	1200	3.0 x 2.6	.12	.03	.28	.42
	1500	2.5 x 2.2	.23	.03	.37	.63
	1800	1.0 x 0.87	.75	.02	.10	.88

TABLE V. RECEIVER LOSS FRACTIONS FOR A 100,000 m^2 FIELD

Absorber Peak Flux (MW/m^2)	Receiver Temp (°C)	Aperture Size (m) W X H	Spillage Loss Fraction	Convective Loss Fraction	Radiative Loss Fraction	Total Receiver Loss Fraction
	600	9.0 x 7.4	.03	.18	.03	.23
	900	8.0 x 6.6	.06	.30	.06	.42
.20	1200	7.0 x 5.8	.11	.42	.11	.65
	1500	6.0 x 4.9	.21	.53	.17	.91
	1800	6.0 x 4.9	.21	.68	.32	(1.21)
	2100	5.0 x 4.1	.40	.76	.38	(1.54)
	600	10.0 x 8.2	.01	.05	.06	.12
	900	9.0 x 7.4	.03	.08	.10	.21
.56	1200	8.0 x 6.6	.06	.11	.16	.33
	1500	7.0 x 5.8	.11	.14	.25	.50
	1800	6.0 x 4.9	.21	.16	.33	.71
	2100	5.0 x 4.1	.40	.18	.38	.97
	600	10.0 x 8.2	.01	.02	.06	.10
	900	9.0 x 7.4	.03	.04	.10	.17
1.0	1200	8.0 x 6.6	.06	.05	.16	.27
	1500	7.0 x 5.8	.11	.05	.24	.41
	1800	6.0 x 4.9	.21	.08	.32	.61
	2100	6.0 x 4.9	.21	.10	.54	.85

TABLE VI. RECEIVER LOSS FRACTIONS FOR A 1,000,000 m^2 FIELD

Absorber Peak Flux (MW/m^2)	Receiver Temp (°C)	Aperture Size (m) W X H	Spillage Loss Fraction	Convective Loss Fraction	Radiative Loss Fraction	Total Receiver Loss Fraction
.25	600	28.5 x 22.8	.04	.16	.04	.24
	900	25.5 x 20.4	.07	.27	.08	.42
	1200	22.5 x 18.0	.13	.38	.15	.66
	1500	21.0 x 16.8	.18	.50	.26	.94
	1800	18.0 x 14.4	.32	.59	.35	(1.26)
	2100	15.0 x 12.0	.49	.65	.42	(1.56)
.62	600	28.5 x 22.5	.04	.04	.07	.15
	900	27.0 x 21.6	.06	.08	.11	.25
	1200	24.0 x 19.2	.10	.11	.18	.39
	1500	21.0 x 16.8	.18	.14	.28	.60
	1800	19.5 x 15.6	.24	.17	.42	.84
	2100	15.0 x 12.0	.49	.18	.42	(1.10)
1.82	600	27.0 x 21.6	.06	.01	.15	.21
	900	25.5 x 20.4	.07	.02	.18	.27
	1200	24.0 x 19.2	.10	.03	.24	.37
	1500	22.5 x 18.0	.13	.03	.35	.51
	1800	19.5 x 15.6	.24	.04	.43	.71
	2100	15.0 x 12.0	.49	.04	.41	.94

TABLE VII. RECEIVER LOSS FRACTIONS AT 1200°C

Field Size (m^2)	Absorber Peak Flux (MW/m^2)	Aperture Size (m) W X H	Spillage Loss Fraction	Convective Loss Fraction	Radiative Loss Fraction	Total Receiver Fraction
10,000	.10	0.5 x 0.44	.85	.28	.01	(1.14)
	.25	3.0 x 2.6	.12	.23	.29	.64
	.45	3.0 x 2.6	.12	.12	.29	.53
	.70	3.0 x 2.6	.12	.07	.29	.48
	1.4	3.0 x 2.6	.12	.03	.28	.42
100,000	.20	7.0 x 5.8	.11	.42	.11	.65
	.27	7.0 x 5.8	.11	.28	.12	.51
	.40	8.0 x 6.6	.06	.18	.16	.39
	.56	8.0 x 6.6	.06	.11	.16	.33
	1.0	8.0 x 6.6	.06	.05	.16	.27
	1.5	8.0 x 6.6	.06	.03	.19	.27
1,000,000	.25	22.5 x 18.0	.13	.38	.15	.66
	.30	24.0 x 19.2	.10	.28	.17	.55
	.43	24.0 x 19.2	.10	.18	.18	.46
	.62	24.0 x 19.2	.10	.11	.18	.39
	1.05	24.0 x 19.2	.10	.06	.20	.36
	1.82	24.0 x 19.2	.10	.03	.24	.37

at a given temperature. System efficiency was calculated by combining the receiver loss fractions with the heliostat field performance. The field performance, as calculated by DELSOL2, is the annual average field efficiency. The receiver thermal loss calculations are design point calculation. Thus, the system efficiency is neither a true annual efficiency nor a true design point efficiency. However, at the higher temperatures, it more accurately represents a design point efficiency. The heliostat field performance of a 50 m^2 heliostat, focused and canted at the slant range, was used to determine the system efficiencies.

The total system efficiency for various receiver temperatures as a function of the peak absorber flux is shown in Figures 16, 17, and 18 for the 10,000 m^2, 100,000 m^2, and 1,000,000 m^2 fields, respectively. As expected, the system efficiency decreases as the receiver temperature increases. At the lower temperatures, there is a definite but broad maximum to the curves. Below about 0.5 MW/m^2, the system efficiency drops as a result of large convective losses. Above about 1.0 MW/m^2, there is a slight decrease in the system efficiency due to the greater radiative losses.

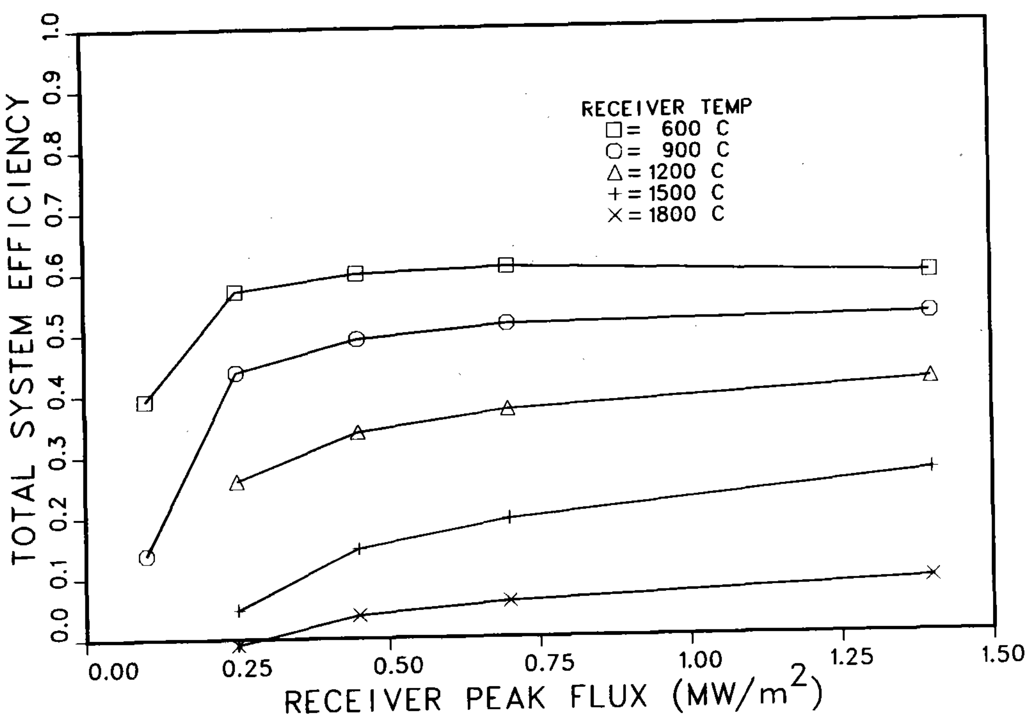

Figure 16. Total System Efficiency for a 10,000 m^2 Field

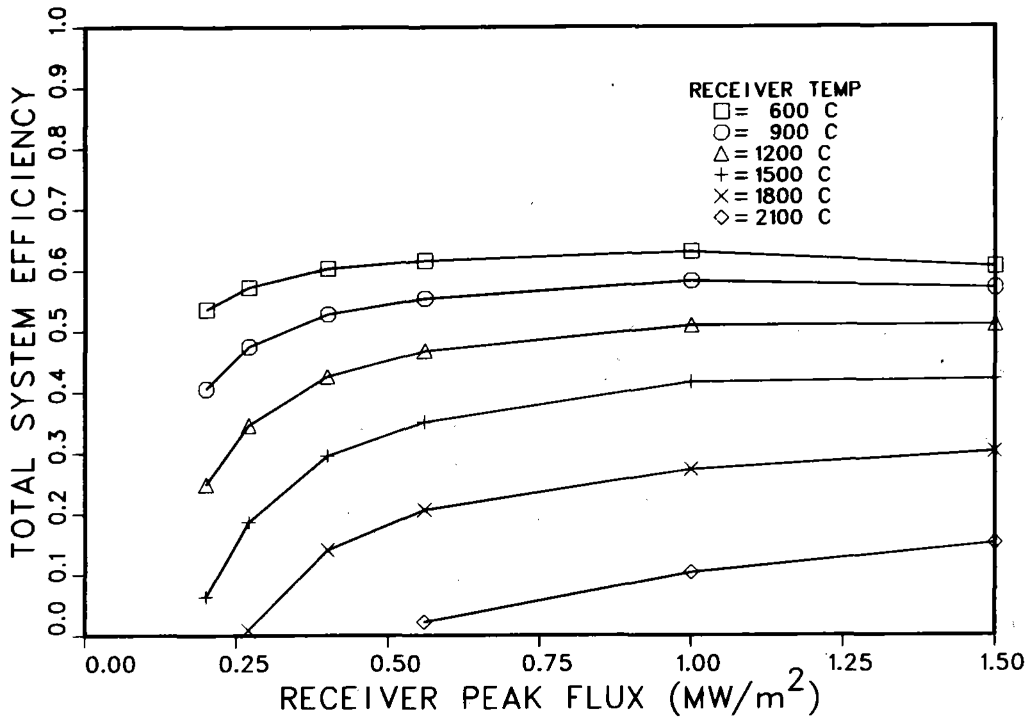

Figure 17. Total System Efficiency for a 100,000 m^2 Field

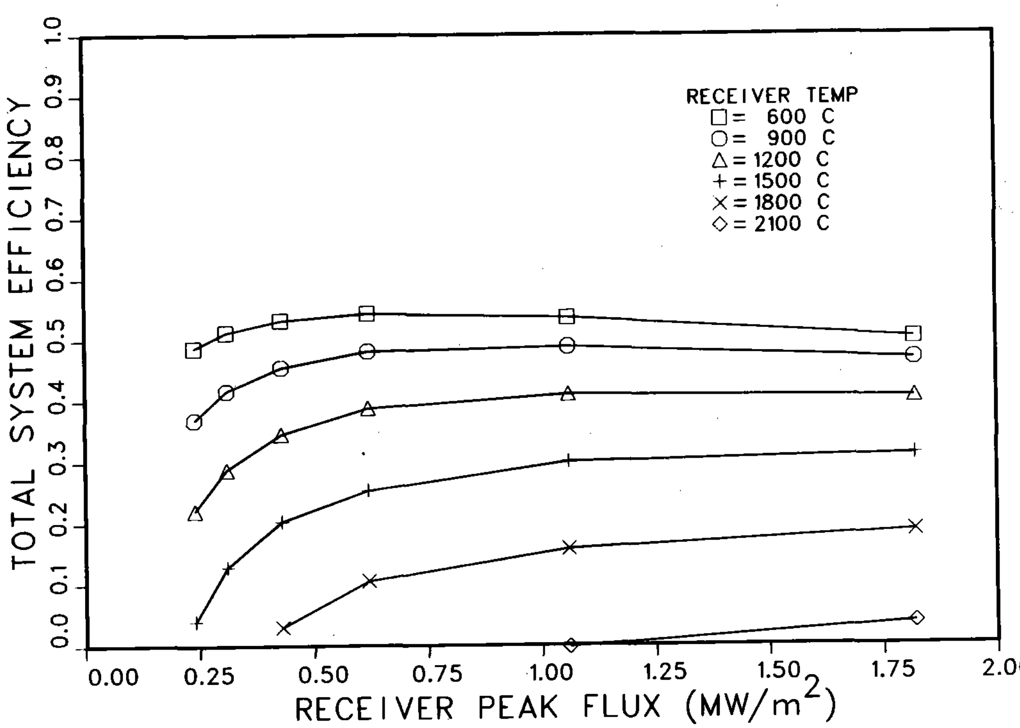

Figure 18. Total System Efficiency for a 1,000,000 m^2 Field

At the higher temperatures, however, the system efficiency increases from some threshold "break-even" flux level to a maximum at the maximum peak flux studied. The maximum flux levels in this study occurred in the smallest receiver sizes, which were chosen from geometrical considerations to be those at which the absorber surface radius was just half of the nominal aperture width. However, the final optimization of the aperture size showed that smaller-than-nominal apertures were desirable at high peak fluxes. Therefore, higher flux (and presumably higher efficiency) cavity receiver designs are possible for these high-temperature cases, although they were not investigated here.

At the 10,000 m^2 field size, receiver temperatures of up to 1800°C are possible, but since the system efficiency is only 9 percent, very little energy is absorbed. At 1200°C, the system efficiency improves to 40 percent, while at 900°C and 600°C the system efficiencies of 50 percent and 60 percent, respectively, are still better. Note that the annual field efficiency excluding spillage (reported in Table II) is 72 percent.

At the 100,000 m^2 field size, the system efficiencies improve over those at the smallest field size, despite a drop in the field performance to 70 percent. At 600°C, the change represents an increase of about 5 efficiency points (0.60 to 0.65). At 900°C, the increase in the system efficiency of 8 efficiency points (0.50 to 0.58) is more significant. As the temperature increases, the improvement in system efficiency for the larger plant becomes even more pronounced.

At the 1,000,000 m^2 field size, the system efficiency is poorer relative to the 100,000 m^2 field size. The decrease is small at the low peak fluxes and more significant (about 10 efficiency points) at higher receiver peak fluxes. This is due to both a decrease in the field performance (6 efficiency points) and a decrease in the receiver performance at the higher receiver peak fluxes.

The high system performance at the 100,000 m^2 field size results from the improvement in receiver performance caused by a smaller ratio of aperture area to heat absorber area for the same peak flux level. At the 10,000 m^2 field size, reductions in the aperture size are limited both by the fact that the sun is not a point source and by the surface and tracking errors in the heliostat model. This fixes the minimum beam size achievable from a heliostat. At the 1,000,000 m^2 field size in a north field configuration, reductions in the aperture size are limited by the divergence of the beams from the farthest heliostats.

Heliostat Size Impact

The above analyses were performed for fields that have a 50 m^2 heliostat focused and canted at the slant range. Changes in the system efficiency resulting from field performance effects (i.e., cosine, shadowing and blocking, and atmospheric attenuation) would be identical to those reported under collector field performance. However, we reinvestigated the effect of heliostat size on the receiver spillage for the smaller aperture sizes dictated by the radiative and convective losses. Receiver spillage as a function of aperture size was calculated by DELSOL2 for 10 m^2 and 100 m^2 heliostats with focusing and canting strategies outlined in the section on collector field performance.

The subsequent reoptimization of the receiver aperture size and receiver performance resulted in only minor changes in the system efficiency. At the 10,000 m^2 field size, a 10 m^2 heliostat with a single focus and cant range of 3 tower heights increased the system efficiency for the highest temperature and highest peak flux system by 6 efficiency points. At the lowest receiver temperature, the increase was slightly over 1 efficiency point. At the 100,000 m^2 field size, changing the heliostat size had almost no effect on spillage and, therefore, on system performance. At the 1,000,000 m^2 field size, both the 50 m^2 heliostat focused and canted at 4 tower heights and the 100 m^2 heliostat focused and canted at the slant range increased the receiver spillage. This resulted in a decrease of less than 4 efficiency points for the highest temperature and peak flux systems and no change in the lower temperature and lower peak flux systems.

Surround Fields

We briefly investigated a four-aperture receiver with a surround heliostat field at the 1,000,000 m^2 field size. The field performance for this configuration increases because of a reduction in spillage losses. However, except at the 600°C receiver temperature, this increased field performance does not make up for the higher receiver thermal losses which result from the larger surface area inherent in the multiple-aperture receiver configuration.

No system performance results are presented for the 100,000 m^2 surround field with a downward-facing aperture, because we were unable to calculate the convective losses from this concept. The convective loss correlation used for the side-facing aperture receivers predicts zero convective losses; we feel this is unrealistic. Although limited tests have been run (Ref. 8 and 9) which directly measure the convective losses from a downward-facing aperture, the method of incorporating these results into the convective loss correlation used in this study is unclear and therefore was not attempted.

Conclusions

The results of this study show that central receiver systems are capable of achieving very high temperatures. However, at the highest temperature studied (2100°C), the best system efficiency for conversion of sunlight to thermal energy is low (15 percent). Temperatures up to 1200°C can be achieved at system efficiencies of 50 percent or greater, while the maximum system efficiencies achievable for receiver temperatures of 1500°C and 1800°C are about 40 percent and 30 percent, respectively.

Table VIII lists the maximum system efficiencies for the three plant sizes studied. Table IX lists their performance at higher temperatures relative to the 600°C receiver temperature. This relative performance value represents the decrease in useful energy collection from a given heliostat field as a result of increasing the receiver temperature. For example, at the 100,000 m^2 field size, the system is capable of converting 63 percent of the incident energy into useful enthalpy gains. Using the incident power listed in Table II, that translates into approximately 69 MW. At 900°C, however, only 92 percent of that amount can be collected, while only 81 percent (about 56 MW) can be collected at 1200°C.

The reciprocal of the relative system performance can be used to closely (but not rigorously) determine the field size increase required to maintain a certain power level when the receiver temperature is increased. For example, at the 100,000 m^2 field size, increasing the receiver temperature to 900°C while maintaining the same power level requires about a 9 percent increase in the field size. At 1200°C the required field size increase is over 23 percent. These results indicate that achieving these very high temperatures does not come cheaply. Whether systems at these high temperatures will be cost-effective is beyond the scope of this study; this question can only be answered by detailed studies of the relative cost and benefits of particular high-temperature systems in a specific application.

The optimum field size for high-temperature central receiver systems appears to be closer to the 100,000 m^2 field size (69 MW_t at 600°C) than to the 1,000,000 m^2 field size (570 MW_t at 600°C). We did not determine exactly where the optimum lies. However, as the receiver temperature is increased, the performance of the 100,000 m^2 field relative to the 1,000,000 m^2 field increases, possibly indicating that the performance of higher temperature systems should optimize at smaller plant sizes.

Open-aperture receiver designs with peak flux levels of less than 0.25 MW/m^2 are very poor performers, especially at temperatures greater than 900°C. Increasing the receiver peak

TABLE VIII

MAXIMUM SYSTEM EFFICIENCIES

Receiver Temperature	10,000 m^2 Field Size	100,000 m^2 Field Size	1,000,000 m^2 Field Size
600°C	.61	.63	.54
900°C	.52	.58	.49
1200°C	.42	.51	.41
1500°C	.26	.42	.31
1800°C	.09	.30	.19
2100°C	--	.15	.05

TABLE IX

RELATIVE SYSTEM PERFORMANCE

Receiver Temperature	10,000 m^2 Field Size	100,000 m^2 Field Size	1,000,000 m^2 Field Size
600°C	1.0	1.0	1.0
900°C	.86	.92	.90
1200°C	.68	.81	.76
1500°C	.43	.67	.57
1800°C	.15	.48	.34
2100°C	--	.24	.09

flux from 0.25 MW/m^2 to 0.5 MW/m^2 at 600^{o}C improves the system performance by over 7 percent. At 900^{o}C this improvement increases to over 15 percent, and at 1200^{o}C the improvement is well over 35 percent. Over 1200^{o}C, the degree of improvement continues to increase.

The results indicate that accommodating high receiver peak fluxes is crucial to achieving high temperatures. High peak fluxes allow a smaller receiver geometry which keeps down the convection losses. Low peak flux levels dictate large receivers with lots of surface area, in order to drive free convection flows.

Recommendations for Future Work

One result of nearly every study of this sort is an increased awareness of those areas in which understanding of, and ability to accurately model, the physical phenomena are weak. Some items that we feel could benefit from either basic research or better modeling techniques are listed below:

- Convective losses from cavity receivers.
  Further research into the convection heat transfer process in cavity receivers is necessary. Specifically, a better understanding is needed of the effect of receiver geometry on the convective heat transfer process.

- Secondary concentrators.
  Although the optics of concentrators are well understood, there is currently no method to easily estimate the improvement in system efficiency that is possible by including a secondary concentrator system.

- Direct absorption receivers.
  If high-temperature receivers are to be built with open apertures, the required high peak absorber flux rates will probably make absorbers constructed from tube sheets difficult to design. The high flux rates create large temperature gradients in the tube sheets, and concomittant high internal stress levels, resulting in substantial materials problems. Direct absorption receivers appear able to eliminate this problem, since the working medium (e.g., solid particle or molten salt) is exposed directly to the solar flux, and no tube-wall temperature gradient is required.

- Aperture windows.
  Closing off the air flow through the aperture without disrupting the incoming radiation would eliminate the convection losses. Solid windows have the problem of radiation absorption, and the

concommitant need for cooling. However, a concept using air windows (or air curtains), which involves blowing a stream of air past the aperture in order to prevent the mixing of the interior gases with the ambient air, has shown some potential.

APPENDIX A--RECEIVER CONVECTIVE LOSS MODELING

The predicted convective losses reported in this paper are based on work done by Kraabel (Ref. 7) at Sandia National Laboratories in Livermore in 1981 and 1982. These results were the most advanced and the most applicable at the time of this study. Kraabel tested a five-sided 2.2 m cube whose open side was vertical. The interior surfaces of the cube were heated to a maximum temperature of about 700°C, which gave a maximum Grashof number (Gr) of about 10^{12}. Kraabel carefully measured and/or calculated the power input and the conductive and radiative losses to arrive at the convective loss. In addition, he measured the velocity and temperature profiles in the "aperture" plane, and from these he was able to generate enthalpy flux profiles.

From the results generated in this configuration, Kraabel was able to deduce the following correlation:

$$Nu = 0.88Gr^{0.33}(T_w/T_a)^{0.18} \qquad (A.1)$$

where Nu is the Nusselt number, and T_w and T_a are the absolute temperatures of the interior walls and the ambient air, respectively. The Grashof number in this correlation was calculated using air properties based on the ambient temperature, and the characteristic length is the height of the absorber surface.

In addition to running tests with the simple cubical configuration, Kraabel also added "lips" which closed off either the bottom third or the top third of the opening. With these lips he was able to vary the ratio of the area of the opening to the area of the interior surfaces, and thus simulate a somewhat more realistic receiver.

His findings for the instances with the lips in place were somewhat surprising. He found that the addition of the bottom lip made essentially no detectable difference in the convective heat transfer. The upper lip, on the other hand, reduced the heat transfer by an amount proportional to the quantity

$$1 - (A_{bot}/A_{tot})^{0.63}$$

where A_{tot} is the total interior surface area, and A_{bot} is the interior surface area below the top of the aperture.

For the situations that he tested, Kraabel found that the overall convective heat transfer coefficient was well correlated by

$$h = 0.81(T_w-T_a)^{0.43}(A_{bot}/A_{tot})^{0.63} \quad \text{(A.2)}$$

where h is the convective heat transfer coefficient in $W/m^2\text{-}^oC$, and is based on the temperatures in ^oC and the total interior area of the cavity in m^2.

Based upon the experimental results, the heat transfer coefficient was found to be independent of cavity size. However, it should be noted that this expression was derived from data taken in the Grashof number range of 10^7 to 10^{12} and has only been verified against independent data in the range 10^6 to 10^9; the values of Gr in this study go as high as 10^{15}.

While we believe that this correlation is the best available model, and for all but one of the receiver geometries which we explored that the correlation is well suited, we feel that much additional work is required to better understand this phenomenon. First, it is not clear that the ratio of A_{bot} to A_{tot} is the best or most general way to characterize the geometry. Consider, for example, a tall narrow cylindrical receiver. Now consider a second receiver which has an identical radius and aperture, but is twice as tall. By changing the height without changing the aperture or the radius, the area ratio has been changed rather substantially, and the correlation would predict significantly different convection losses. However, since the air in the top of the receiver is likely to be stagnant (or, at worst, interacting only with itself), it is not intuitively clear that there would actually be any change in the convective heat transfer.

Another potential weakness in the form of this correlation is that it does not account for other geometric factors which intuitively appear important. For example, Kraabel's tests do not examine the importance of the aspect ratio of the cavity (the ratio of the depth of the cavity to its height). Nor did he test directly the effect of tilting the aperture toward the ground. For example, for a downward-facing aperture, the current form of the correlation would predict no convective loss for this receiver geometry (A_{bot} = 0). In our opinion, there should almost certainly be some convective heat loss because it is unlikely that the air volume inside the cavity would be completely stagnant.

Thus the area of convective losses from cavity receivers still presents some major questions. In general, there is little or no understanding of the sophisticated mechanisms which are at work in this situation. As a result, the use of Kraabel's correlation (or any other calculational technique currently available) should ideally be limited to geometries which are close to those on which they are based. This must remain a caveat on the results and conclusions presented in this report.

REFERENCES

1. "Solar Repowering/Industrial Retrofit Program Element Plan," U.S. Department of Energy San Francisco Operations Office.

2. J. D. Fish, P. De Laquil III, S. E. Faas, and C. L. Yang, "Central Receiver Steam Systems for Industrial Process Heat Applications," Sandia National Laboratories, SAND81-8223, April 1981.

3. P. De Laquil III, C. L. Yang, and J. E. Noring, "Solar Central Receiver High Temperature Process Air Systems," Sandia National Laboratories, SAND82-8254, February 1983.

4. T. A. Dellin, M. A. Fish, and C. L. Yang, "A User's Manual For DELSOL2: A Computer Code For Calculating the Optimal System Design For Solar Thermal Central Receiver Plants," Sandia National Laboratories, SAND81-8237, August 1981.

5. M. Abrams, "RADSOLVER--A Computer Program for Calculating Spectrally-Dependent Radiative Heat Transfer in Solar Cavity Receivers," Sandia National Laboratories, SAND81-8248, September 1981.

6. A. F. Emery, "Instruction Manual for the Program 'Shapefactor'," Sandia National Laboratories, SAND80-8027, October 1980.

7. D. L. Siebers and J. S. Kraabel, "Estimating Convective Energy Losses From Solar Central Receivers," Sandia National Laboratories, SAND84-8717, April 1984.

8. "One-Fourth Megawatt Solar Receiver Final Report," Sanders Associates, Inc., DOE/ET/21011-1, October 1979.

9. P. Le Quere, F. Penot, and M. Mirenayat, "Experimental Study of Heat Loss Through Natural Convection from an Isothermal Cubic Open Cavity," Convective Losses from Solar Central Receivers: Proceedings of a DOE/SERI/SNLL Workshop, P. K. Falcone, ed., Sandia National Laboratories, SAND81-8014, October 1981.

UNLIMITED RELEASE

INITIAL DISTRIBUTION

UC-62e (243)

U. S. Department of Energy
Forrestal Building
1000 Independence Avenue, S. W.
Washington, D.C. 20585
Attn: H. Coleman
C. Carwile
K. Cherian
C. Mangold
M. Scheve
T. Wilkins

U. S. Department of Energy
P. O. Box 5400
Albuquerque, NM 87115
Attn: G. Pappas
J. Weisiger

U. S. Department of Energy
1333 Broadway
Oakland, CA 94612
Attn: R. Hughey
G. Katz
W. Lambert

University of California
Department of Electrical and
Computer Engineering
Davis, CA 95616
Attn: M. Soderstrand

University of Houston
Solar Energy Laboratory
4800 Calhoun
Houston, TX 77704
Attn: A. Hildebrandt

Aerospace Corporation
2350 El Segundo Blvd.
El Segundo, CA 90245
Attn: P. Munjal

ARCO Power Systems
7061 S. University, Suite 300
Littleton, CO 80122
Attn: F. Blake
D. Gorman

Arizona Public Service Company
P. O. Box 21666
Phoeniz, AZ 85036
Attn: J. McGuirk
E. Weber

Babcock and Wilcox
91 Stirling Avenue
Barberton, OH 44203
Attn: G. Grant
I. Hicks
D. Smith

Badger Energy, Inc.
One Broadway
Cambridge, MA 02142
Attn: C A. Bolthrunis

Bechtel Group, Inc.
P. O. Box 3965
San Francisco, CA 94119
Attn: G. W. Braun
J. Darnell
P. DeLaquil III (15)

Black and Veatch Consulting Engineers
P. O. Box 8405
Kansas City, MO 64114
Attn: J. C. Grosskreutz
J. E. Harder

Boeing Engineering and Construction Company
P. O. Box 3707
Seattle, WA 98124
Attn: R. B. Gillette

Burns & McDonnell
P. O. Box 173
Kansas City, MO 64141
Attn: M. Soderstrum

California Energy Commission
1111 Howe Avenue, MS-70
Sacramento, CA 95825
Attn: D. Pierson

Combustion Engineering, Inc.
1000 Prospect Hill Road
Windsor, CT 06095
Attn: C. R. Buzzuto

DFVLR
Apartado 19, Tabernas
Almeria, Spain
Attn: M. Becker

El Paso Electric Company
P. O. Box 982
El Paso, TX 79946
Attn: J. E. Brown

Electric Power Research Institute
P. O. Box 10412
Palo Alto, CA 94303
Attn: E. DeMeo

Foster Wheeler Development Co.
12 Peach Tree Hill Road
Livingston, NJ 07039
Attn: S. F. Wu
R. Zoschak

Georgia Institute of Technology
Atlanta, GA 30332
Attn: C. T. Brown

Gibbs and Hill, Inc.
393 Seventh Avenue
New York, NY 10001
Attn: J. J. Jimenez

Institute of Gas Technology
Suite 218
1825 K. Street, N. W.
Washington, D. C. 20036

Martin Marietta
P. O. Box 179, L#0450
Denver, CO 80201
Attn: T. Heaton
T. Tracey

McDonnell Douglas
5301 Bolsa Avenue
Huntington Beach, CA 92647
Attn: C. Finch
L. W. Glover

Olin Chemicals Group
P. O. Box 2896
Lake Charles, LA 70624
Attn: J. Morgan

Olin Chemicals Group
120 Long Ridge Road
Stamford, CT 06904
Attn: F. N. Christopher
L. C. Fiorucci

Pacific Gas and Electric Company
3400 Crow Canyon Road
San Ramon, CA 94526
Attn: C. Weinberg

Pacific Northwest Laboratory
P. O. Box 999
Richland, WA 9932
Attn: B. Johnson
S. Hauser

Public Service Company of New Mexico
P. O. Box 2267
Albuquerque, NM 87103
Attn: A. Akhil

Rockwell International
Energy Systems Group
8900 De Soto Avenue
Canoga Park, CA 91304
Attn: T. Springer
A. Z. Ullman

Solar Energy Industries Association
1156 15th Street, NW
Suite 520
Washington, D.C. 20005
Attn: C. LaPorta

Solar Energy Research Institute
1617 Cole Boulevard
Golden, CO 804011
Attn: J. Anderson (20)
M. Murphy
L. Shannon

Southern California Edison
P.O. Box 800
Rosemead, CA 92807
Attn: J. N. Reeves
P. Skvarna
R. S. Williamson

Stearns-Roger
P.O. Box 5888
Denver, CO 80217
Attn: W. R. Lang

Stone and Webster Engineering Corporation
P. O. Box 1214
Boston, MA 02107
Attn: R. W. Kuhr

Westinghouse Electric Corporation
Advanced Energy Systems Division
P.O. Box 10864
Pittsburgh, PA 15236
Attn: J. R. Maxwell

D. G. Schueler, 6220
J. V. Otts, 6222
R. S. Claassen, 8000; Attn: D. M. Olson, 8100
A. N. Blackwell, 8200
D. L. Hartley, 8300
C. S. Selvage, 8000A
C. Hartwig, 8124
M. E. John, 8125
J. Kraabel, 8132
R. L. Rinne, 8220
8400; Attn: R. A. Baroody, 8410
A. G. Schuknecht, 8420
H. Hanser, 8440
J. F. Barham, 8460
J. B. Wright, 8450
A. C. Skinrood, 8452
D. N. Tanner, 8452
J. C. Swearengen, 8453 (25)
J. B. Woodard, 8454
Publications Division 8265/Technical Library Processes Division, 3141
Technical Library Processes Division, 3141 (3)
M. A. Pound, 8424, for Central Technical Files (3)

Org.	Bldg.	Name	Rec'd by	Org.	Bldg.	Name	Rec'd by
6226		Jim Muir					

Sandia National Laboratories